LAWRENCE
LIVERMORE
NATIONAL
LABORATORY

LLNL-JRNL-815880

Groundwater noble gas measurements confirm paleorecharge hypotheses at Pahute Mesa, Nevada National Security Site, Nevada, USA

A. Visser, E. Kwicklis, I. Farnham, A. Tompson, R. Hershey

October 21, 2020

Hydrogeology Journal

Disclaimer

This document was prepared as an account of work sponsored by an agency of the United States government. Neither the United States government nor Lawrence Livermore National Security, LLC, nor any of their employees makes any warranty, expressed or implied, or assumes any legal liability or responsibility for the accuracy, completeness, or usefulness of any information, apparatus, product, or process disclosed, or represents that its use would not infringe privately owned rights. Reference herein to any specific commercial product, process, or service by trade name, trademark, manufacturer, or otherwise does not necessarily constitute or imply its endorsement, recommendation, or favoring by the United States government or Lawrence Livermore National Security, LLC. The views and opinions of authors expressed herein do not necessarily state or reflect those of the United States government or Lawrence Livermore National Security, LLC, and shall not be used for advertising or product endorsement purposes.

Using groundwater noble gas measurements to confirm paleorecharge hypotheses at Pahute Mesa, Nevada National Security Site, Nevada, USA

Ate Visser,* Edward Kwicklis, Irene Farnham, Andrew F.B. Tompson, and Ronald L. Hershey

*: Corresponding author: visser3@llnl.gov

Abstract

Pahute Mesa (Nevada, USA) was the site of 85 underground nuclear tests between 1965 and 1992 whose residual radiochemical inventory poses a contaminant threat to local groundwater resources. To assess the fate and transport of these radionuclides in groundwater, several geochemical studies, including this one, have been conducted to understand long-term groundwater flow patterns at, and downgradient of, Pahute Mesa. Groundwater samples from the Pahute Mesa area at the Nevada National Security Site were analyzed for noble gases ($^{3}He/^{4}He$ isotopic ratio and He, Ne, Kr, Ar and Xe concentrations) to infer groundwater recharge temperatures and provide additional evidence in support of groundwater flow patterns and the presence of late-pluvial Pleistocene groundwater. These data confirm recent findings (based on groundwater geochemistry and isotope compositions) that most recharge in the area occurred under temperature conditions much cooler than are found today, except near major drainages where ephemeral runoff continues to recharge shallow groundwater. These noble gas data indicate that noble gas recharge temperatures and terrigenic He components have been re-set where groundwater has flowed upward over barriers formed by caldera margins, or near the regional discharge area (Oasis Valley) where shallow groundwater has interacted with shallow

soil gas. This evidence from groundwater noble gas measurements, in combination with other isotopic and geochemical studies, supports the current understanding of the unusual hydrogeology and recharge history of Pahute Mesa.

Key Words: Geochemistry, groundwater isotopes, noble gases, nuclear test site, USA

1. Introduction

1.1 Understanding the Hydrogeology of Pahute Mesa

Pahute Mesa at the Nevada National Security Site (NNSS) in the USA, formerly the Nevada Test Site, was the location of 85 underground nuclear tests between 1965 and 1992, some with explosive yields exceeding an equivalent of 1-Megaton trinitrotoluene (TNT) (U.S. DOE/NNSA, 2015)(Fig. 1). There is a considerable inventory of residual radioactivity associated with these tests that pose a contamination threat to local groundwater resources (Finnegan, et al., 2016). To assess the fate and transport of these radionuclides in groundwater and support safe groundwater management of the atomic legacy, numerous hydrogeological and mass transport studies have been performed since the 1970s (e.g. Winograd and Thordarson, 1975; Tompson et al., 2002). To provide a more complete understanding of long-term, historical flow patterns than can be provided by hydraulic data alone, a number of groundwater geochemical and isotopic studies

(Thomas et al., 2002; Kwicklis et al., 2005; Rose et al., 2006; Navarro, 2020; Kwicklis et al., 2021) have been conducted for the Pahute Mesa-Oasis Valley (PM-OV) groundwater system defined by Fenelon et al. (2016). These studies used the spatial variability in relatively conservative constituents such as Cl^- and SO_4^{2-}, together with variations in the stable isotopes of hydrogen (δ^2H) and oxygen ($\delta^{18}O$), as the basis for identifying flow directions and estimating groundwater mixing ratios.

The present study complements the earlier aforementioned groundwater geochemical and isotopic studies, particularly those of Kwicklis et al. (2021), by calculating groundwater noble gas recharge temperatures (NGRT) from the PM-OV groundwater flow system. In the context of these earlier studies, it was evaluated whether groundwater recharge occurred under the present climate or during the late Pleistocene, when pluvial climates with much wetter and cooler conditions prevailed. The evidence for the dominance of pluvial recharge in the Pahute Mesa area groundwater is based largely on the much lighter stable isotopic composition of groundwater compared to modern winter precipitation or high-elevation perched-spring discharge and the offset of these data from the present-day meteoric water line, combined with corrected dissolved inorganic carbon (DIC) ^{14}C ages for the groundwater (see Kwicklis et al., 2021).

Dissolved noble gases in groundwater provide independent evidence for the conditions under which recharge took place, including water-table fluctuations (Cey, et al., 2008, Ingram, et al., 2007, Visser, et al., 2018) and the water-table temperature (Cey, et al., 2009), allowing for the reconstruction of past climates (Aeschbach-Hertig, et al., 2000, Mazor, 1972, Stute, et al., 1995,

60 Stute, et al., 1992). Additionally, the elevation of mountain-block recharge can be estimated
61 (Hershey et al., 2007, Manning and Solomon, 2005, Peters, et al., 2018). The isotopic ratios of
62 heavier noble gases can be used to derive the depth of the water table below the surface based on
63 the isotopic fractionation caused by gravitational settling (Seltzer, et al., 2017). Secondary re-
64 equilibration complicates the interpretation of dissolved noble gases but can also provide
65 evidence for gas ebullition from groundwater (Blicher-Mathiesen, et al., 1998, Visser, et al.,
66 2009) or shallow flow over groundwater barriers (Thomas, et al., 2003).

67 *1.2. Previous and Related Work*

68 A related paper (Kwicklis et al., 2021) summarizes new interpretations of groundwater flow in
69 the PM-OV groundwater flow system based on recently acquired groundwater geochemical and
70 isotopic data from new and existing wells located in, and south of, the Pahute Mesa testing areas
71 (Fig. 2). The data from this relatively small area were analyzed in the context of more regional
72 studies conducted by Thomas et al. (2002), Rose et al. (2006) and Kwicklis et al. (2005) to
73 provide new insights into the PM-OV groundwater flow system. Among the key findings from
74 the Kwicklis et al. (2021) study is that steep gradients in groundwater Cl^- and SO_4^{2-} are caused
75 by the confluence of two distinct parts of the flow system: (1) more saline groundwater flowing
76 southward from the vicinity of Gold Flat dry lake playa (located north of Pahute Mesa, Fig. 2);
77 and (2) dilute groundwater flowing westward from high-elevation recharge areas on Pahute and
78 Rainier Mesa or possibly the Kawich Range (Fig. 2). Both the more saline and dilute parts of the
79 flow system were interpreted to be dominantly of pluvial origin based on the very light δ^2H and
80 $\delta^{18}O$ of the groundwater relative to modern, volume-weighted mean winter precipitation

(Moscati and Scofield, 2011) or high-elevation perched-spring discharge (Ingraham et al., 1991), and the calculated ^{14}C ages of the groundwater (Kwicklis, 2009). The DIC ^{14}C age of the high salinity groundwater ranges from 15 ka to 18 ka. The dilute groundwater flowing west from eastern Pahute Mesa is also late Pleistocene groundwater based on its DIC ^{14}C age. The high salinity groundwater is associated with wind-borne ocean salts in precipitation (as indicated by ^{36}Cl) deposited near Gold Flat playa and concentration of sulfate from runoff and groundwater discharge (as indicated by $\delta^{34}S$) as it alternately filled and dried out in the late Pleistocene (Kwicklis et al., 2021) and not from upwelling of deep hydrothermal fluids or water-rock reactions with geothermal minerals within the calderas. The persistence of late pluvial groundwater for both the dilute and saline parts of the flow system is attributed to long unsaturated-zone travel times of the dilute component through the thick (> 600 m) vadose zone beneath Pahute Mesa, and low groundwater flux of the high salinity groundwater and high porosity of the basin fill in Gold Flat. The mixed groundwater flows through the Thirsty Canyon area and ultimately toward Oasis Valley, where it mixes with other groundwater from eastern Pahute Mesa and elsewhere near the discharge area (Kwicklis et al., 2005).

1.3 Purpose and Scope

The purpose of this study was to determine if and where Pahute Mesa area recharge temperatures estimated from noble gas data were consistent with a paleo origin for the groundwater. These data were collected over several decades for an area larger than the recent study area considered by Kwicklis et al. (2021), but far smaller than the area considered by the regional studies described in Thomas et al. (2002), Rose et al. (2006), and Kwicklis et al. (2005). The

interpretations from the noble gas data are made in the context of the flow system understanding developed based on other data such as Cl^-, SO_4^{2-}, δ^2H, $\delta^{18}O$, and DIC $\delta^{13}C$ and ^{14}C, but also provide an additional independent check on those interpretations.

2. Methods

2.1 Noble Gases as Groundwater Tracers

The primary sources of noble gases — helium (He), neon (Ne), argon (Ar), krypton (Kr), and xenon (Xe) — dissolved in natural waters are equilibration with the atmosphere and/or the decay of several radioactive isotopes (Ozima and Podosek, 2002). The abundances of the heavier noble gases (Ne, Ar, Kr, Xe) in groundwater are caused primarily by atmospheric equilibration of water during groundwater recharge and excess-air formation (bubble entrainment near the water table caused by water-level fluctuations), and their elemental abundances are directly related to the temperature and altitude of the groundwater recharge location (Manning and Solomon, 2005; Plummer et al., 2001; Rademacher et al., 2001 and 2005; Singleton and Moran, 2010). In rare cases, rapid recharge in fractured aquifers results in noble gas signatures in groundwater that still reflects the typical composition found in snow and ice (Amalberti et al., 2018; Niu et al., 2017; Warrier et al., 2012)

The solubility of noble gases depends on the temperature of the air-water interface and the salinity of the solution. Heavier noble gases (Kr and Xe) are more sensitive to temperature than lighter noble gases (He and Ne). The equilibrium solubility concentrations of noble gases dissolved in groundwater reflect the conditions at the water table, in terms of temperature, salinity, and

(partial) pressure. Because the proportions of noble gases in the atmosphere are constant, partial pressures depend on the atmospheric pressure at the elevation of the water table. While depletion of oxygen in the unsaturated zone can result in higher partial pressures of noble gases at the water table (Hall et al., 2012), dissolved oxygen concentrations in Pahute Mesa groundwater (4.1±1.5 mg/L, $\mu\pm\sigma$, n=34) suggest that oxygen depletion in the vadose zone before groundwater recharge is negligible. Barometric pumping in deep unsaturated zones at both Pahute Mesa and Yucca Mountain has been documented and evaluated with respect to transport of radionuclide gases from underground nuclear tests (e.g. Carrigan et al., 1996; Sun et al., 2016) and geologic storage of radioactive waste (e.g., Bourret et al., 2020; Feldman et al., 2020; Harp et al., 2020; Bourret et al., 2019; Jordan et al., 2015; Thorstenson et al., 1998; Sullivan and Pescatore, 1994). With barometric pumping, air flows into and out of the unsaturated zone during atmospheric pressure highs and lows. At Pahute Mesa, gas flow is primarily through large aperture interconnected factures in volcanic rocks (Bourret et al., 2020) maintaining high oxygen concentrations at the water table.

Water-table fluctuations can cause bubble entrapment and (partial) dissolution resulting in a phenomenon called “excess air,” defined as concentrations of noble gases in excess of atmospheric equilibrium. The “excess-air” contribution can be corrected for using concentration measurements of all atmospheric noble gases. If the water-table elevation is known, the exact recharge temperature can then be derived from the dissolved noble gas concentrations. Because noble gases are each transported conservatively in groundwater, their ratios along flow paths downgradient from the recharge areas do not change because of differences in their transport velocity.

Unlike the several hundred meter deep water tables at Pahute Mesa, the water table is near the surface in most hydrogeologic settings, and air pressure at the land surface can be used to approximate the recharge gas pressure. In these cases, the water-table temperature is also close to the mean annual air temperature at the surface (Cey et al., 2008). Under these conditions, NGRTs can accurately reconstruct past climatic conditions (Aeschbach-Hertig et al., 2000; Stute et al., 1995; Stute et al., 1992; Mazor 1972).

If recharge occurs at an elevation more than 100 meters above the well elevation, the recharge elevation (which determines the atmospheric pressure at the water table) needs to be estimated prior to calculating the NGRT. If water tables are shallow, recharge is typically assumed to occur at the mean annual air temperature. The atmospheric lapse rate (~6 °C decrease per kilometer elevation gain) can then be used constrain the elevation and temperature at which recharge may have occurred. This principle has been used to study mountain block recharge (Hershey et al., 2007, Manning and Solomon, 2005) and high elevation recharge on Mount Shasta, California (Peters et al., 2018).

In the Pahute Mesa area of the NNSS, none of the assumptions typically made in other recharge studies using noble gases are likely to be valid. Because of the rugged topography and lateral groundwater flow toward lower elevation discharge areas, recharge can occur at much higher elevations than the surface elevation at the location that groundwater was sampled. Under present-day conditions, water tables are up to several hundred meters below the land surface. Because of the geothermal gradient (typically 33 °C increase per kilometer depth in the unsaturated zone at Pahute Mesa), temperatures at the water table can be tens of degrees

Centigrade warmer than the land surface. Elevation and temperature are, therefore, no longer constrained by the atmospheric lapse rate. Recharge also may have occurred under past climate conditions, possibly colder and wetter than present, which results in different water-table depths and temperatures at the land surface. Additionally, prior research in southern Nevada (Thomas et al., 2003) demonstrated that focused shallow groundwater flow over geological barriers can cause re-equilibration of noble gas concentrations with vadose zone gases. This re-equilibration effectively resets the noble gas thermometer and uncouples the noble gas concentrations from the recharge conditions. Given these complicating factors, noble gases dissolved in groundwater need to be compared carefully with present-day conditions when investigating groundwater recharge timing and flow patterns at the NNSS.

He isotopes (^{3}He and ^{4}He) in groundwater are derived from several different sources: equilibration with the atmosphere (^{3}He and ^{4}He); excess air from bubble entrainment in the unsaturated zone (^{3}He and ^{4}He) (Schlosser et al., 1989); nuclear fission of lithium-6 (^{6}Li) (nucleogenic ^{3}He); production of ^{4}He by uranium (U)-thorium (Th) decay (radiogenic ^{4}He); mantle He (^{3}He and ^{4}He); and ^{3}H decay (tritiogenic ^{3}He) (Tolstikhin and Kamensky, 1969). "Terrigenic He" refers to the combined He contribution from nucleogenic, radiogenic, and mantle sources. The concentration of the dissolved He is related to the age of the sample, increasing with time since last contact with the atmosphere because of the accumulation of terrigenic He. Mantle ^{3}He is easily detected because the isotopic ratio ($^{3}He/^{4}He$) of mantle He (~8 times atmospheric) is distinctly different from the isotopic ratio of radiogenic He (~1 percent of atmospheric). Patterns of terrigenic He were examined to support the interpretation of noble gas re-equilibration.

Underground nuclear tests are known to introduce noble gas isotopes to the vadose zone and groundwater inventory (Kersting, 1996), including short-lived and stable isotopes of xenon (e.g. Sun et al., 2016), ^{85}Kr, and ^{3}He as the stable product of test-derived ^{3}H. Because the analysis here is limited to groundwater samples with no detectable test-derived tritium (with the exception of two samples with elevated ^{3}He), test-derived noble gas isotopes are not present in this dataset.

2.2 Noble Gas Data from Pahute Mesa and Vicinity

This study was focused on a set of groundwater samples collected from wells on Rainier Mesa and Pahute Mesa, and wells located in the Thirsty Canyon area (labeled ER-EC) between the NNSS and Oasis Valley (Fig. 3 and Table S1 in the electronic supplementary material ESM1). Samples were collected using submersible groundwater pumps. Noble gas analyses were performed at Lawrence Livermore National Laboratory on an automated multi-port mass spectrometry system with multiple reactive metal getters and three cryotraps. Helium isotopes were analyzed using a VG-5400 noble gas mass spectrometer equipped with an electron multiplier. Neon, krypton and xenon concentrations were measured using a quadrupole mass spectrometer via isotope dilution with isotopically enriched ^{22}Ne, ^{86}Kr and ^{136}Xe. The Ar concentration is determined by pressure measurement using a high-sensitivity capacitance manometer. A detailed description of the analytical procedure is provided in ESM2. The isotope spike and pressure measurements preclude the routine analysis of the isotopic ratios. The procedure was calibrated using water samples equilibrated with the atmosphere at a known temperature and air standards spiked with known quantities of the noble gases. Analytical

uncertainties are 1% for $^{3}He/^{4}He$, 2% for He, Ne, and Ar, and 3% for Kr and Xe. Prior to the automation and installation of the isotope spike and RGA in 2003, Xe was routinely analyzed manually on the VG5400, and Ne and Kr for select samples only. For these "historical" samples, the same analytical uncertainty has been assumed.

The quality control (QC) process used to identify outliers in the noble gas data and select the final noble gas data set for the Pahute Mesa area is described in ESM2. For Pahute Mesa, noble gas data from 37 locations (springs, wells, or multilevel wells) were included in this paper (Fig. 3). Forty-two analyses from Pahute Mesa were available for interpretation of the NGRT and terrigenic He content.

Noble gas concentrations were fitted to the unfractionated excess air (UA) model according to Visser et al (2016), assuming the well water table as the recharge elevation. Fits for samples with only two atmospheric noble gas analyses were accepted although the probability of the fit could not be calculated. The uncertainty of the estimated derived parameters (e.g. noble gas recharge temperature, ΔNe) was based on the propagation of the analytical uncertainty of the noble gases following Ballentine and Hall (1999). Samples with He isotope ratios impacted by subsurface nuclear tests – as evidenced by elevated tritium concentrations in these samples – were excluded from the terrigenic He interpretation.

Two additional conceptual models, diffusive and closed-system re-equilibration, were explored to gain a better understanding of possible re-equilibration and mixing processes. These conceptual models are described in detail in ESM2. The reduced number of parameters that are

necessary to constrain the UA model allowed us to include a larger number of samples (with fewer than four atmospheric noble gas measurements) and expand the spatial coverage and hydrogeological insights. The apparent NGRT and excess air component derived from the simplified UA model still provide reliable indicators of whether sample has been affected by re-equilibration at a higher temperature.

2.3 Hydrogeology of Pahute Mesa

Oligocene to Miocene volcanic rocks erupted from at least seven calderas in the Pahute Mesa area within the southwestern Nevada volcanic field (Blankennagel and Weir, 1973; Sawyer et al., 1994; Grauch et al., 1999). Calderas in the Pahute Mesa area include the Silent Canyon caldera complex made up of the Area 20 and Grouse Canyon calderas, the Timber Mountain caldera complex made up of the Ammonia Tanks and Rainier Mesa calderas, the Black Mountain Caldera, Redrock Valley Caldera, and the Claim Canyon Caldera (Fig.2). Volcanic rocks from the calderas are more than 3,000 m thick include rhyolitic-to-dacitic lava flows; ash-flow and ash-fall tuffs; and breccias (Winograd and Thordarson, 1975; Laczniak et al., 1996; Faunt et al., 2010; Blankennagel and Weir, 1973; Sawyer et al., 1994). Quaternary volcanism within the southwestern Nevada volcanic field is outside of the PM-OV groundwater flow system.

Intrusion of granitic stocks accompanied Tertiary volcanism in the Pahute Mesa area, exposed along the southeast and north edges of the Timber Mountain resurgent dome (Sinnock et al, 1982). A massive granitic intrusion in the volcanic rocks at the northwestern corner of the NTS was encountered at a depth of about 9000 ft (2.7 km) in exploratory drill hole PM2, the remnant

248 heat of which causes a high geothermal gradient and elevated water table temperatures to this
249 day. Other Tertiary granitic stocks are inferred to occur below the Timber Mountain Caldera
250 (Sinnock et al, 1982).

251 Pahute Mesa itself is the westward-dipping, erosional remnant of a once more extensive volcanic
252 plateau located in the far northwest corner of the NNSS (Fig. 1; Winograd and Thordarson,
253 1975). Eighty-five nuclear tests were conducted underground in zeolitic tuffs underlying Pahute
254 Mesa and an additional 61 nuclear tests were conducted in tunnels and shafts in tuff formations
255 underlying Rainier Mesa, directly to the east of Pahute Mesa (NNSA/NFO, 2015). Rainier Mesa
256 includes the highest elevation areas on the NNSS and, in an area of strongly elevation-dependent
257 precipitation and net infiltration, probably has some of the largest net infiltration on the NNSS.
258 Groundwater recharge on Rainer Mesa, and other high elevation areas in southern Nevada,
259 occurs mainly from melting of winter snow (Hershey et al., 2008; Ingraham et al. ,1991) with
260 little recharge from summer rains (Winograd et al., 1998; Winograd and Riggs, 1984), in part,
261 because much of the NNSS lies in a deficit annual average precipitation region (French, 1983).
262 Much of the infiltration on Rainier Mesa may be diverted laterally to the west as perched water
263 flowing above low-permeability zeolitic tuffs; eventually the perched and regional groundwater
264 systems merge and groundwater from Rainier Mesa flows southward beneath Fortymile Canyon
265 (Fig. 1), westward into Pahute Mesa, and possibly to areas north of the NNSS (Hershey et al.,
266 2008; DOE, 2018). Shallow groundwater beneath Fortymile Canyon is dominated by local
267 modern recharge from ephemeral runoff based on its high DIC ^{14}C activity (> 70 pmc), its
268 relatively heavy stable isotope composition, and the measured water table rises in shallow wells
269 following runoff events (Middleton et al., 2019; Kwicklis et al., 2021). In contrast, the Thirsty

Canyon drainage in western Pahute Mesa does not appear to be as hydrologically active as Fortymile Canyon, based on the very light groundwater $\delta^{2}H$ and $\delta^{18}O$ compared to modern precipitation and the low DIC ^{14}C activity of the groundwater. This may be because of the lower elevation and lower precipitation in western Pahute Mesa compared with the eastern Pahute Mesa. Maps of net infiltration based on daily water-balance calculations presented in Middleton et al. (2019) and summarized in Kwicklis et al. (2020) show relatively small rates of net infiltration on Timber Mountain because of clayey soil, as well as negligible net infiltration in lower elevation areas covered by thick porous alluvium, which stores shallow infiltration in the root zone until it can be removed by evapotranspiration.

The unsaturated zone beneath most of Pahute Mesa is more than 600 m thick. It is estimated that it takes more than 10,000 years for present-day net infiltration to reach the water table given the relatively low rates of infiltration estimated for higher elevation areas on Pahute Mesa (5 to 10 mm/yr), (Middleton et al., 2019; Kwicklis et al., 2021). The deep water tables, combined with the geothermal gradient, result in water-table temperatures that exceed the mean annual air temperature by several degrees centigrade, with implications for dissolved noble gas concentrations at the water table in equilibrium with the vadose zone gas phase.

Groundwater movement at, and downgradient of, Pahute Mesa is mostly through volcanic rocks. The volcanic rocks include welded and non-welded tuffs and lava flows. The non-welded, originally vitric tuffs tend to be altered to zeolites where they have been submerged beneath the water table. The welded tuffs tend to form extensive ash-flow sheets, whereas the lavas are associated with local vents and tend to fill paleo-valleys. The lateral continuity of each of these

rock types is disrupted by hydrostratigraphic offsets across caldera boundaries, faults and structural zones.

The welded tuffs and lavas have been conceptualized as being the principal aquifers and the zeolitic tuffs have been conceptualized as confining units, but there is substantial overlap and considerable variability in the hydraulic properties of the different rock types (Frus and Halford, 2018; Garcia et al., 2017; Fenelon et al., 2016), calling into question the existence of a well-defined hydrostratigraphy at Pahute Mesa (Mirus et al., 2016). For all rock types, the primary permeability of the rock matrix is very low and water movement and bulk-permeability are dominated by the presence and interconnectedness of fractures and faults near the well.

The groundwater hydraulic-head contours for the PM-OV groundwater flow system are superimposed on a map of structural features at the water table in Fig. 2. The groundwater contours suggest that groundwater from high-elevation areas at Rainier Mesa and eastern Pahute Mesa spreads out radially to the northwest, west or southwest, with the northwest component of flow eventually turning southwest along a series of faults in the Area 20 caldera. Groundwater east of the Ammonia Tanks Caldera flows south from Rainier Mesa along Fortymile Canyon. Hydraulic gradients in western Pahute Mesa within the Area 20 caldera indicate convergent flow within a hydraulic trough that appears to be associated with either the Purse and West Purse Fault or the Thirsty Canyon Lineament (TCL) on the west, and the West Boxcar Fault on the east. As represented in Fig. 2, hydraulic gradients appear to be relatively flat beneath Timber Mountain and steepen dramatically in areas south of the Claim Canyon Caldera. Timber Mountain is assumed to be part of the southern boundary of the PM-OV groundwater flow

system provided there are low-permeability rocks restricting flow beneath the mountain or sufficient recharge to create a groundwater (Jackson et al., 2021; Hershey et al., 2020; Fenelon et al., 2016; Fenelon et al. (2010). Although no wells exist beneath Timber Mountain to confirm the presence of either low-permeability rocks or a recharge mound, these features could contribute to the re-orientation of flow from Pahute Mesa around the northwest margin of Timber Mountain. Alternatively, hydraulic-head contours steepen toward the southern boundary of the map area suggesting that north–south flow from Pahute Mesa beneath Timber Mountain may be precluded by structural and stratigraphic features to the south of Timber Mountain, perhaps associated with the Claim Canyon Caldera as opposed to features associated with the Timber Mountain caldera complex (TMCC) itself. This interpretation is also based upon the observation that similarly steep hydraulic gradients do not exist along the northern boundary of the TMCC. Because groundwater movement could be blocked by barriers directly south of Timber Mountain, groundwater from Pahute Mesa may dam up north of the barrier and flow around the northwest side of Timber Mountain toward lower Beatty Wash and Oasis Valley.

The area southwest of Area 20 is defined by major faults and caldera structural features. Formations in this area have been down-dropped along the east–west trending Northern Timber Mountain Moat Structure Zone. This area, referred to as “the Bench” (Fig. 2) is of particular interest because radionuclide-contaminated groundwater has been observed to be migrating through this area and off the NNSS. Although migrating off the NNSS, radionuclide contamination is still confined to government land within the Nevada Test and Training Range (NTTR) boundary (Fig. 2).

2.4 Present-Day Water-Table Conditions

Water-table temperatures are available for a subset of Pahute Mesa area wells from Reiner (2007) and associated data bases. Water table temperatures for more recently drilled wells (ER-EC-11 through -15, and ER-18-2) were obtained from the well completion reports. Additionally, mean annual air temperatures from PRISM were analyzed in the context of the geothermal gradient (PRISM, 2016). Land-surface elevations are as high as 2300 m above mean sea level at Rainier Mesa, gradually decreasing toward Pahute Mesa (1,700 to 2,150 m), Thirsty Canyon (ER-EC wells) (1,300 to 1,800 m), and Oasis Valley (1,000 to 1,300 m). Variation in the regional water-table elevation is smaller, with water tables ranging from 1,300 m at Rainier Mesa to 1,050 m at Oasis Valley. On Rainier Mesa, perched water tables in volcanic aquifers thought to contribute to Pahute Mesa area groundwater are found at elevations as high as 1,850-m. Because the water table is relatively flat compared to the land surface, water-table depths largely follow the topographic relief, ranging from several meters in Oasis Valley to more than 600 m at Pahute Mesa. As a result of the deep water tables and the natural geothermal gradient (Fig. 4), water-table temperatures vary from near 20 °C below the thin vadose zone of Oasis Valley (where surface air temperatures are highest) to nearly 40 °C under the thick vadose zone of Pahute Mesa (where surface air temperatures are lower). Wells with water tables deeper than 300 m below ground surface show a consistent geothermal gradient of 33 °C per kilometer, calculated as the difference between the PRISM mean annual air temperature (PRISM, 2016) and the temperature 1.5 m below the water table (Reiner, 2007). Wells with shallower water tables, particularly at Oasis Valley, show a higher geothermal gradient.

Seven groups of observed water-table temperatures were identified (Fig. 4). Because of the large geothermal gradient in the vadose zone, higher water-table temperatures are observed at wells with deeper (lower) water tables. Because water tables are shallower in Oasis Valley, water-table temperatures are lower and closer to the mean annual air temperature, despite the overall increase in mean annual air temperature with decreasing elevation. Perched water tables at 1,850 m on Rainier Mesa are close to 20 °C (Group 1) and between 21 °C and 23 °C at 1,600 m elevation (Group 2). On Pahute Mesa, water-table elevations at the sampling locations cluster around the 1,400 to 1,450 m and 1,325 to 1,375 m elevations, with corresponding temperatures between 25 °C and 32 °C (Group 3) and between 28 °C and 34.5 °C (Group 4). Water tables in the Thirsty Canyon area (the ER-EC wells) range from 31 °C to 52 °C at elevations between 1,200 m and 1,300 m (Group 5). Oasis Valley water-table temperatures range from 18.5 °C to 24 °C at elevations between 1,100 m and 1,250 m (Group 6). A seventh potential recharge equilibrium location is the Gold Flat playa lake that was periodically present in the Pleistocene (Group 7). Evidence of lake levels constrain the elevation to around 1,555 m, and the mean annual air temperature at this elevation is estimated to be 11.3 °C at present but was probably lower in the Pleistocene. If Pleistocene recharge north of Pahute Mesa took place at higher elevations than Gold Flat playa, recharge temperatures could have been either higher or lower than 11.3 °C depending on the surface elevation and water-table depth.

While the perched Rainier Mesa water-table temperatures overlap with the Oasis Valley water-table temperatures, and the range in Pahute Mesa water-table temperatures is large, characterizing present-day water-table conditions helps to identify likely recharge sources and distinguish between recent and Pleistocene recharge. Samples that show NGRTs within the range

of temperatures encompassed by these groups may have recharged under present-day climatic conditions or re-equilibrated at flow barriers. Groundwater with a lower NGRT has most likely recharged under prior climatic conditions.

2.5 Recharge and Re-Equilibration Scenarios

Given the measured water-table temperatures at the sampling locations, four possible scenarios are presented that could explain the observed NGRTs. In some cases, the appropriate scenario for a given well cannot be distinguished by the noble gas data alone but must be interpreted in the context of other data such as stable isotopes or mixing ratios suggested by conservative anions. Generally, $\delta^{18}O$ in precipitation tends to become lighter with elevation (although considerable variation in the lapse rate exists across the NNSS and can constrain the elevation where recharge water originated once evaporative fractionation, possible paleoclimate influences, and the potential for runoff from high-elevation areas have been considered. The four potential categories for classifying the NGRTs are as follows:

Scenario 1: Groundwater recharge occurred under Pleistocene climate conditions. NGRT will be lower than present-day water-table temperatures at the sampling location or potential upgradient recharge locations, including Gold Flat playa lake with present-day mean annual air temperature of 11.3 °C. The $\delta^{18}O$ of groundwater will reflect Pleistocene precipitation, which is lighter than present-day precipitation (Kwicklis et al., 2021).

Scenario 2: Recharge occurred locally under present-day (Holocene) climatic and water-table conditions. As a result, NGRTs are close to the present-day water-table temperatures at the sample location. The groundwater $\delta^{18}O$ reflects present-day precipitation, which is isotopically heavier than Pleistocene recharge.

Scenario 3: Groundwater is focused over shallow geological barriers that cause re-equilibration of NGRTs at present-day water-table conditions (discussed in detail below). NGRTs upgradient of the flow barrier will reflect recharge conditions, while NGRTs downgradient of the flow barrier will reflect present-day water-table conditions. Because the source of recharge in this scenario does not change across the flow barrier, the $\delta^{18}O$ on either side of the flow barrier will be the same.

Scenario 4: Groundwater is a mixture of various recharge sources. Measured dissolved noble gas concentrations and $\delta^{18}O$ of groundwater are mixtures between the two end-members. Ranges of NGRTs and $\delta^{18}O$ will be correlated along a mixing line.

Re-equilibration of noble gases from groundwater has been observed previously at flow barriers at Frenchman Flat (Thomas et al., 2002). A loss of CO_2 from groundwater was attributed to higher temperatures and lower hydrostatic pressures at shallow geological flow barriers. Similar conditions along Rainier Mesa, Pahute Mesa, Thirsty Canyon (ER-EC wells), and Oasis Valley groundwater flow paths can cause re-equilibration of noble gases, effectively resetting the noble gas thermometer. Although degassing of CO_2 has not been observed at Pahute Mesa, re-equilibration of DIC ^{14}C with soil gas is suspected to cause younger apparent DIC ^{14}C ages in

shallow Oasis Valley wells (White and Chuma, 1987). Additionally, the presence of a geothermal anomaly (i.e. exceptionally high groundwater temperatures at depth) and upward gradients can upwelling of deeper groundwater towards the water table. These conditions have been observed in exploratory drill holes PM-2 and UE-20J, west of the Silent Canyon caldera, where a geothermal gradient of 43.3°C per kilometer in PM-2 was attributed to remnant heat in a massive granitic intrusive body that was penetrated below a depth of 8,400 feet (Blankennagel et al., 1973).

3. Results

In this section, measured noble gas concentrations (Table S2 of ESM1) and derived parameters (i.e., NGRT, excess air, terrigenic He, Table S3 of ESM1) at individual wells are interpreted in the context of present-day conditions and the possible recharge and re-equilibration scenarios. NGRTs are mapped spatially and in a geological cross section to distinguish patterns of flow and the timing of recharge.

3.1 Evaluation of Noble Gas Recharge Temperatures (NGRT)

NGRTs were evaluated considering the physical and geochemical characteristics of the Rainier Mesa, Pahute Mesa, Thirsty Canyon, and Oasis Valley groundwater flow systems and the four process scenarios described previously. Because the elevation of the perched water table at Rainier Mesa and the water table at Pahute Mesa vary by 500 m at present, air pressure at the water table and, consequentially, the equilibrium noble gas concentrations vary by 6 percent.

This difference in pressure corresponds to a change in NGRT of 1.75 °C. To account for this subtle sensitivity, NGRTs were evaluated at their water-table elevation.

Five groups of recharge and/or re-equilibration conditions can be distinguished (Fig. 6). In Fig. 6, the symbol shape indicates the general sample location, and the symbol color indicates the NGRT group into which the sample falls. The present-day water-table elevations and temperature boxes are plotted for reference. The noble gas temperatures are listed in Table 1, along with the grouping and interpretation of the NGRT.

3.2 Hydrogeologic Interpretation of NGRT Results

This section presents the spatial distribution of NGRT, along with the measured present-day water-table temperatures and $^{3}He/^{4}He$ ratios and concentrations. As shown in Fig. 6, the NGRT estimates for all Pahute Mesa and Bench area samples upgradient of the TMCC are observed to be much cooler than the present-day water-table temperatures at the sample sites. This is true of both the high-concentration Cl^- and SO_4^{2-} groundwater samples from along the western boundary of the NNSS and the more dilute groundwater samples further east that were inferred to be derived from recharge in higher elevation areas in eastern Pahute Mesa and perhaps Rainier Mesa (Kwicklis et al., 2021). However, the coolest NGRT estimates in central Pahute Mesa are cooler than even the present-day water-table temperatures at Rainier Mesa, supporting the paleo-recharge scenario even if the dilute groundwater originated exclusively from Rainier Mesa.

The groundwater downgradient of the Bench in the TMCC has NGRTs close to present-day water-table temperatures. Because the $\delta^{2}H$ and $\delta^{18}O$ data of these TMCC area samples are nearly

identical to the upgradient groundwater with cooler NGRTs, the preferred interpretation for the TMCC groundwater is that upwelling of groundwater along the TMCC boundary resulted in re-equilibration of the cooler NGRT with present-day temperatures at the water table. The high groundwater temperatures observed in ER-EC-15 (50 °C at the water table increasing to 64 °C at 975 m depth) were an indication for upwelling of deep groundwater against a flow barrier. ER-EC-15 is located close to the major fault, the West Purse Fault (Fig. 2). Note that $\delta^{18}O$ for ER-EC-15 is consistent with other Pahute Mesa groundwater and does not show a geothermal isotopic shift that would suggest upwelling of deep geothermal water along this fault. However, terrigenic He concentrations are elevated (up to 128 times equilibrium) with isotopic ratios above radiogenic He production ratios suggesting a substantial component of mantle He.

A secondary re-equilibration of NGRT occurred downgradient of the TMCC toward Oasis Valley, where low-permeability clastic rocks force groundwater to the surface in a series of springs and seeps, bringing groundwater into contact with shallow soil gas. As discussed in Kwicklis et al. (2021), this same process resulted in groundwater exchange with DIC $^{14}CO_2$ in the soil gas near Oasis Valley, resetting the DIC ^{14}C ages without a significant shift in the $\delta^{2}H$ and $\delta^{18}O$. The NGRTs of ER-OV-01 and ER-OV-03c are interpreted to be in a transition between the re-equilibrated NGRT of the TMCC and Oasis Valley areas. Their relatively high NGRTs compared to water-table temperatures could be the result of a second ongoing, but incomplete, re-equilibration at shallower and colder groundwater-table conditions at the downgradient edge of the TMCC. This suggests there are no deep continuous groundwater flow paths from Pahute Mesa into and out of the TMCC.

The NGRT of groundwater at ER-EC-07 is also in equilibration with the present-day water-table temperature, although in this case, the much heavier groundwater δ^2H and $\delta^{18}O$ and young DIC ^{14}C age suggest the low NGRT of the sample (21.7 °C) probably reflects high-elevation recharge from Timber Mountain (the measured water sample temperature was 30 °C). The same is probably true for the ER-30-1 and UE-29a#2 samples, which receive runoff and recharge from Fortymile Canyon (Fig. 1) based on observed water-table rises following run-off events, their heavier δ^2H and $\delta^{18}O$ values, and young DIC ^{14}C age (Kwicklis et al., 2021). The water samples at nearby ER-30-1 and UE-29a#2 had NGRTs of 22.6 and 19.0 °C, respectively, close to the measured sample temperatures of 23.6 and 22.5 °C, and their origin is interpreted to be local present-day recharge (Table 3). ER-18-2 is a similar example, although a local geothermal anomaly causes a much higher water-table and recharge temperature (46.2°C and 63.6 °C).

Fig. 7 shows a cross section of NGRT and present-day water-table temperatures extending from Rainier Mesa on the right side of the figure to Oasis Valley on the left side. NGRTs are plotted at the midpoints of the open intervals (represented by black bars), and water-table temperatures are plotted at the water table. The plot highlights (1) the much cooler NRGTs compared with water-table temperatures beneath Rainier and Pahute Mesa; (2) the similar NRGTs and present-day water-table temperatures beneath the TMCC and Oasis Valley; and (3) the transitional NRGTs between the TMCC and Oasis Valley areas, which is evident at ER-OV-01 and ER-OV-06a.

Re-equilibration of noble gases at the water table is expected to reset the excess air component to zero ($\Delta Ne = 0\%$). However, most samples with elevated noble gas temperatures, indicative of re-equilibration, still contain a significant component of excess air, up to 78%. Plotting excess air

(ΔNe) against noble gas temperatures (Fig. 8) shows that all samples fall within a mixing envelope (dashed red lines) between the range of water table temperatures observed in Thirsty Canyon (EC) wells and the samples with the highest excess air components found at Pahute Mesa (over 200%). This suggests that these groundwater samples contain a mixture of completely re-equilibrated groundwater (ΔNe=0% and high NGT) and undisturbed groundwater (high ΔNe and low NGT). Incomplete re-equilibration is less likely because the lighter noble gases (which are more sensitive to excess air) are more diffusive than the heavier noble gases (which are more sensitive to temperature). Incomplete re-equilibration would therefore result in a larger reset of the excess air component and a limited shift in the derived noble gas temperature. The secondary re-equilibration from Thirsty Canyon to Oasis Valley results in a further reduction in the excess air component, this time accompanied by a shift towards lower noble gas temperatures.

Terrigenic He concentrations and isotopic ratios (Fig. 9) support the hypothesis of noble gas re-equilibration across flow boundaries such as the TMCC. Isotopic ratios for terrigenic He are not available for many samples on Pahute Mesa because of the addition of nuclear test-derived ^{3}He. Terrigenic He at Rainier Mesa and Pahute Mesa is predominantly of radiogenic (natural U/Th decay) origin, with isotopic ratios below 0.2 times atmospheric. Increases in the concentration of terrigenic He and elevated isotopic ratios are observed west of Pahute Mesa. Across the TMCC boundary, isotopic ratios remain elevated, but He concentrations decrease, indicating re-equilibration with vadose zone gases. Further downgradient toward Oasis Valley, the concentration and isotopic ratio increase further to approach those of atmospheric gases or mantle He. Evidence for a secondary re-equilibration of noble gases toward Oasis Valley is not

as pronounced. Tolicha Peak groundwater contains terrigenic He of radiogenic origin but at very low concentrations. Because of these low concentrations, mixing of flow paths from TMCC toward Oasis Valley with groundwater from Tolicha Peak would likely retain the TMCC signature of terrigenic He.

4. Summary and Conclusions

In summary, NGRTs in groundwater beneath Pahute Mesa are consistently much cooler than present-day water-table temperatures and reflect recharge under Pleistocene climate conditions. Elevated noble gas temperatures in the Thirsty Canyon area (ER-EC wells) are thought to be a result of re-equilibration because they show a $\delta^{18}O$ signature similar to Pleistocene recharge (Fig. 10). In contrast to wells at Pahute Mesa and in the Thirsty Canyon area (ER-EC wells), wells in the Fortymile Canyon area show evidence for local recharge and noble gas temperatures that reflect present-day water-table temperatures. A good example is ER-EC-7, where the NGRT (21.7 °C) is close to the measured water-table temperature (23.1 °C), and the $\delta^{18}O$ value (-13.2 ‰) indicates a local present-day source.

These data independently confirm recent findings, based on groundwater geochemistry and isotope compositions, that most recharge in the area occurred under temperature conditions much cooler than are found today, except near major drainages where ephemeral runoff continues to recharge shallow groundwater, and that there is not significant upwelling of geothermal waters in the PM-OV groundwater system. Noble gas recharge temperatures (NGRT) and terrigenic He components have been re-set where groundwater has flowed over barriers formed by caldera

538 margins, or near the regional discharge area (Oasis Valley) where shallow groundwater has
539 interacted with shallow soil gas. These groundwater noble gas measurements provide an
540 additional line of evidence, independent of other geochemical or isotopic tracers, that supports a
541 better understanding of the unusual and complex hydrogeology and recharge history of Pahute
542 Mesa.

543 ## 5. Acknowledgements

544 On behalf of all authors, the corresponding author states that there is no conflict of interest. This
545 work was performed under the auspices of the U.S. Department of Energy by Lawrence
546 Livermore National Laboratory under Contract DE-AC52-07NA27344. LLNL-JRNL-815880

547

6. References

Aeschbach-Hertig W, Peeters F, Beyerle U, Kipfer R (2000) Palaeotemperature reconstruction from noble gases in ground water taking into account equilibration with entrapped air. Nature 405: 1040

Amalberti, J., Hall, C.M. and Castro, M.C. (2018) Noble gas signatures in snow: A new experimental investigation. Chem. Geol., Volume 483, p275-285, https://doi.org/10.1016/j.chemgeo.2018.02.022

Ballentine CJ, Hall CM (1999) Determining paleotemperature and other variables by using an error-weighted, nonlinear inversion of noble gas concentrations in water. Geochimica Et Cosmochimica Acta 63: 2315-2336 DOI DOI: 10.1016/S0016-7037(99)00131-3

Blankennagel RK, Weir JE Jr (1973) Geohydrology of the Eastern Part of Pahute Mesa, Nevada Test Site, Nye County, Nevada, Professional Paper 712-B. Denver, CO: US Geological Survey

Blicher-Mathiesen G, McCarty GW, Nielsen LP (1998) Denitrification and degassing in groundwater estimated from dissolved dinitrogen and argon. Journal of Hydrology 208: 16-24

Bourret SM, Kwicklis EM, Harp DR, Ortiz JP, Stauffer PH, 2020. Beyond Barnwell: Appling lessons learned from the Barnwell sit to other historic underground nuclear tests at Pahute Mesa to understand radioactive gas-seepage observations. Journal of Environmental Radioactivity 222: 106297

566 Bourret SM, Kwicklis EM, Miller TA, Stauffer PH, 2019. Evaluating the importance of
567 barometric pumping for subsurface gas transport near an underground nuclear test site. Vadose
568 Zone Journal 18:180134

569 Carrigan CR, Heinle RA, Hudson GB, Nitao JJ, Zucca JJ (1996) Trace gas emissions on
570 geological faults as indicators of underground nuclear testing. Nature 382: 528

571 Cey BD, Hudson GB, Moran JE, Scanlon BR (2008) Impact of Artificial Recharge on Dissolved
572 Noble Gases in Groundwater in California. Environ Sci Technol 42: 1017-1023

573 Cey BD, Hudson GB, Moran JE, Scanlon BR (2009) Evaluation of Noble Gas Recharge
574 Temperatures in a Shallow Unconfined Aquifer. Ground Water 47: 646-659

575 Faunt, CC, Sweetkind DS, Belcher WR (2010) Three-dimensional Hydrogeologic Framework
576 Model, *in* Belcher WR, Sweetkind DS, eds., chap. E *of* Death Valley Regional Ground-water
577 Flow system, Nevada and California—Hydrogeologic Framework and Transient Ground-water
578 Flow Model, Professional Paper 1711 Reston, VA: US Geological Survey p 161–249

579 Feldman J, Paul M, Xu G, Rademacher DX, Wilson J, Nenoff, TM, 2020. Effects of natural
580 zeolites on field-scale geologic noble gas transport. Journal of Environmental Radioactivity 220-
581 221:106279

582 Fenelon JM, Sweetkind DS, Laczniak RJ (2010) Groundwater Flow Systems at the Nevada Test
583 Site, Nevada: A Synthesis of Potentiometric Contours, Hydrostratigraphy, and Geologic
584 Structures, Professional Paper 1771 Reston, VA: US Geological Survey

585 Fenelon JM, Halford KJ, Moreo MT (2016) Delineation of the Pahute Mesa–Oasis Valley
586 Groundwater Basin, Nevada, Version 11, Scientific Investigations Report 2015-5175 Carson
587 City, NV: US Geological Survey

588 Finnegan DL, Bowen MS, Thompson JL, Miller CM, Baca PL, Olivas LF, Geoffrion CG, Smith
589 DK, Goishi W, Esser BK, Meadows JW, Namboodiri N, Wild JF (2016) Nevada National
590 Security Site Underground Radionuclide Inventory,1951-1992: Accounting for Radionuclide
591 Decay through September 30, 2012, LA-UR-16-21749, Los Alamos National Laboratory, NM.

592 French, RH (1983) Precipitation in Southern Nevada. Journal of Hydraulic Engineering
593 107:1023-1035

594 Frus RJ, Halford KJ (2018) Documentation of Single-Well Aquifer Tests and Integrated
595 Borehole Analyses, Pahute Mesa and Vicinity, Nevada, Scientific Investigations Report 2018-
596 5096 Reston, VA: US Geological Survey

597 Garcia, CA, Jackson TR, Halford KJ, Sweetkind DS, Damar NA, Fenelon JM, Reiner SR (2017)
598 Hydraulic Characterization of Volcanic Rocks in Pahute Mesa Using an Integrated Analysis of
599 16 Multiple-Well Aquifer Tests, Nevada National Security Site, 2009–14, Scientific
600 Investigations Report 2016-5151. Carson City, NV: US Geological Survey

601 Grauch VJS, Sawyer, DA, Fridrich CJ, Hudson MR (1999). Geophysical Framework of the
602 Southwestern Nevada Volcanic Field and Hydrogeologic Implications, Professional Paper 1608,
603 Denver, CO: US Geological Survey

604 Hall, C.M., Castro, M.C., Lohmann, K.C. and Sun, T. (2012) Testing the Noble Gas
605 Paleothermometer with a Year-long Study of Groundwater Noble Gases in an Instrumented
606 Monitoring Well. Water Resources Research, vol. 48, W04517, doi:10.1029/2011WR010951

607 Harp, DR, Bourret SM, Stauffer, PH, Kwicklis EM, 2020. Discriminating Underground Nuclear
608 Explosions Leading to Late-Time Radioactive Gas Seeps. Geophysical Research Letters
609 10.1029/2019GL086654

610 Hershey RL, Paces JB, Singleton MJ, Kwicklis EM, Decker DL, Fryer WM, and Earman S
611 (2008) Geochemical and Isotopic Evaluation of Groundwater Movement in Corrective Action
612 Unit 99: Rainier Mesa and Shoshone Mountain, Nevada Test Site, DOE/NV/26383-10;
613 Publication No 45229 Las Vegas, NV: Desert Research Institute

614 Hershey, RL, Heilweil, VM, Gardner, P, Lyles, BF, Earman, S, Thomas, JM, and Lundmark,
615 KW (2007) Ground-water Chemical Interpretations Supporting the Basin and Range Regional
616 Carbonate-rock Aquifer System (BARCAS) Study, Eastern Nevada and Western Utah.
617 Publication No 41230 Reno, NV: Desert Research Institute

618 Hershey RL, Parashar R, Cooper CA, Heintz KM, Pham HV, Lyles BF (2020) Evaluation of
619 Timber Mountain Recharge and Groundwater Flow in Relation to Pahute Mesa-Oasis Valley

Flow System, DOE/NV/0003590-56; Publication No 45294 Las Vegas, NV: Desert Research Institute.

Ingraham NL, Lyles BF, Jacobson RL, Hess JW (1991) Stable Isotopic Study of Precipitation and Spring Discharge in Southern Nevada, Journal of Hydrology, 125(3-4):243–258

Ingram RGS, Hiscock KM, Dennis PF (2007) Noble Gas Excess Air Applied to Distinguish Groundwater Recharge Conditions. Environmental Science & Technology 41: 1949-1955 DOI 10.1021/es061115r

Jackson, T.R., Fenelon, J.M., and Paylor, R., 2021, Groundwater Flow Conceptualization of the Pahute Mesa–Oasis Valley Groundwater Basin, Nevada: A synthesis of Geologic, Hydrologic, Hydraulic-Property, and Tritium Data: U.S. Geological Survey Scientific Investigations Report 2020–5134, plate 1. https://doi.org/10.3133/sir20205134.

Jordan AB, Stauffer PH, Knight EE, Rougier E, Anderson DN, 2015. Radionuclide gas transport through nuclear explosion-generated fracture networks. Scientific Reports 5:18383.

Kersting A (1996) The State of the Hydrologic Source Term, Lawrence Livermore National Laboratory, CA (United States) UCRL-ID-126557.

Kwicklis, EM, Rose TP, Benedict FC Jr (2005) Evaluation of Groundwater Flow in the Pahute Mesa–Oasis Valley Flow System Using Groundwater Chemical and Isotopic Data, LA-UR-05-4344. Los Alamos, NM: Los Alamos National Laboratory

638 Kwicklis E (2009) Appendix D: Evaluation of Groundwater Travel Times in the PM-OV Flow
639 System from 14C Data" In Phase I Transport Model of Corrective Action Units 101 and 102:
640 Central and Western Pahute Mesa, Nevada Test Site, Nye County, Nevada, S-N/99205--111. Las
641 Vegas, NV: Stoller-Navarro Joint Venture

642 Kwicklis E, Farnham I, Hershey RL, Visser A, Hoaglund J (2021) Understanding long-term
643 groundwater flow at Pahute Mesa and vicinity, Nevada National Security Site, USA, from
644 naturally occurring geochemical and isotopic tracers. Hydrogeology Journal DOI
645 10.1007/s10040-021-02397-x

646 Manning, A.H., and D.K. Solomon. 2005. "An Integrated Environmental Tracer Approach To
647 Characterizing Groundwater Circulation in a Mountain Block." In Water Resources Research,
648 Vol. 41(12).

649 Marine, I.W. 1979. "The Use of Naturally Occurring Helium To Estimate Groundwater
650 Velocities for Studies of Geologic Storage of Radioactive Waste." In Water Resources Research,
651 Vol. 15(5): pp.1130–1136.

652 Marty, B., and A. Jambon. 1987. "C/3He in Volatile Fluxes from the Solid Earth: Implication for
653 Carbon Geodynamics." In Earth and Planetary Science Letters, Vol. 83: pp. 16–26.

654 Mazor E (1972) Paleotemperatures and other hydrological parameters deduced from noble gases
655 dissolved in groundwaters; Jordan Rift Valley, Israel. Geochimica et Cosmochimica Acta 36:
656 1321

Mirus, B.B., K.J. Halford, D.S. Sweetkind, J.M. Fenelon, 2016. Testing the suitability of geologic frameworks for extrapolating hydraulic properties across scales, Hydrogeology Journal (24) p. 1133-1146.

Moscati RJ, Scofield KM (2011) Meteoric Precipitation at Yucca Mountain, Nevada: Chemical and Stable Isotope Analyses, 2006–09 US Geological Survey Scientific Investigations Report 2011-5140, 16 p

Navarro (2020) Phase II Geochemical and Isotopic Evaluation of Groundwater Flow in the Pahute Mesa–Oasis Valley Flow System, Nevada, Rev 0, N0002653-069, Las Vegas, NV

Niu, Y., Castro, M., Hall, C.M., Gingerich, S.B., Scholl, M.A. and Warrier, R.B. (2017) Noble gas signatures in the Island of Maui, Hawaii: Characterizing groundwater sources in fractured systems. Water Resources Research, 53(5), pp.3599-3614.

NNSA/NFO, see US Department of Energy, National Nuclear Security Administration Nevada Field Office

Ozima, M., and F.A. Podosek. 2002. Noble Gas Geochemistry, Second Edition. Cambridge, UK: Cambridge University Press.

PRISM, see PRISM Climate Group.

673 Peters, E., A. Visser, B. Esser, and J. Moran. 2018. “Tracers Reveal Recharge Elevations,
674 Groundwater Flow Paths and Travel Times on Mount Shasta, California.” In Water, Vol. 10(2):
675 p.97.

676 Planavsky, N., C.A, Partin, and A. Bekker. 2011. “Carbon Isotopes as a Geochemical Tracer.”
677 InEncyclopedia of Astrobiology: pp. 241–245. Berlin, Heidelberg, Germany: Springer.

678 Plummer, L.N., E. Busenberg, J.K. Böhlke, D.L. Nelms, R.L. Michel, and P. Schlosser. 2001.
679 “Groundwater Residence Times in Shenandoah National Park, Blue Ridge Mountains, Virginia,
680 USA: A Multi-Tracer Approach.” In Chemical Geology, Vol. 179(1–4): pp. 93–111.

681 PRISM Climate Group. 2016. “PRISM Climate Data.” Corvallis, OR: Northwest Alliance for
682 Computational Science & Engineering at Oregon State University. As accessed at
683 http://prism.oregonstate.edu.

684 Rademacher, L.K., J.F. Clark, G.B. Hudson, D.C. Erman, and N.A. Erman. 2001. “Chemical
685 Evolution of Shallow Groundwater as Recorded by Springs, Sagehen Basin; Nevada County,
686 California.” In Chemical Geology, Vol. 179(1–4): pp. 37–51.

687 Rademacher, L.K., J.F. Clark, D.W. Clow, and G.B. Hudson. 2005. “Old Groundwater Influence
688 on Stream Hydrochemistry and Catchment Response Times in a Small Sierra Nevada
689 Catchment: Sagehen Creek, California.” In Water Resources Research, Vol. 41(2).

690 Reiner, S.R. 2007. Ground-Water Temperature Data, Nevada Test Site and Vicinity, Nye,
691 Clark,andLincoln Counties, Nevada, 2000–2006, Data Series 269. Carson City, NV:
692 U.S.Geological Survey.

693 Reiner SR, Laczniak RJ, DeMeo GA, Smith JL, Elliott PE, Nylund WN, Fridrich CJ (2002)
694 Ground-Water Discharge Determined from Measurements of Evapotranspiration, Other
695 Available Hydrologic Components, and Shallow Water-Level Changes, Oasis Valley, Nye
696 County, Nevada, Water-Resources Investigations Report 01-4239 Carson City, NV: US
697 Geological Survey

698 Rose TP, Benedict FC Jr, Thomas JM, Sicke WS, Hershey RL, Paces JB, Farnham IM, and
699 Peterman ZE (2006) Geochemical Data Analysis and Interpretation of the Pahute Mesa–Oasis
700 Valley Groundwater Flow System, Nye County, Nevada, August 2002, UCRL-TR-224559
701 Livermore, CA: Lawrence Livermore National Laboratory

702 Sawyer DA, Fleck RJ, Lanphere MA, Warren RG, Broxton DE, Hudson MR (1994) Episodic
703 Caldera Volcanism in the Miocene Southwestern Nevada Volcanic Field: Revised Stratigraphic
704 Caldera Framework, 40Ar/39Ar Geochronology, and Implications for Magmatism and Extension
705 In Geological Society of America Bulletin, 106(10):1304–1318.

706 Schlosser, P., M. Stute, H. Dorr, C. Sonntag, and K.O. Münnich. 1988. “Tritium/3He Dating of
707 Shallow Groundwater.” In Earth and Planetary Science Letters, Vol. 89(3-4): pp. 353–362.

708 Schlosser, P., M. Stute, C. Sonntag, and K.O. Münnich. 1989. “Tritiogenic 3He in Shallow
709 Groundwater.” In Earth and Planetary Science Letters, Vol. 94(3–4): pp. 245–256.

710 Seltzer AM, Severinghaus JP, Andraski BJ, Stonestrom DA (2017) Steady state fractionation of
711 heavy noble gas isotopes in a deep unsaturated zone. Water Resources Research 53: 2716-2732

712 Singleton, M.J., and J.E. Moran. 2010. “Dissolved Noble Gas and Isotopic Tracers Reveal
713 Vulnerability of Groundwater in a Small, High-Elevation Catchment to Predicted Climate
714 Changes.” In Water Resources Research, Vol. 46(10): pp. W00F06.

715 Sinnock, S., 1982. Geology of the Nevada Test Site and nearby areas, southern Nevada. Sandia
716 National Laboratories.

717 SNJV, see Stoller-Navarro Joint Venture

718 Solomon, D.K. and E.A. Sudicky. 1991. “Tritium and He-3 Isotope Ratios for Direct Estimation
719 of Spatial Variations in Groundwater Recharge.” In Water Resources Research, Vol.27(9):
720 pp.2309–2319.

721 Stoller-Navarro Joint Venture (2009) Phase I Transport Model of Corrective Action Units 101
722 and 102: Central and Western Pahute Mesa, Nevada Test Site, Nye County, Nevada, Rev 1, S-
723 N/99205--111 Las Vegas, NV

Stute M, Clark JF, Schlosser P, Broecker WS, Bonani G (1995) A 30,000 yr Continental Paleotemperature Record Derived from Noble Gases Dissolved in Groundwater from the San Juan Basin, New Mexico. Quaternary Research 43: 209

Stute M, Schlosser P, Clark JF, Broecker WS (1992) Paleotemperatures in the Southwestern United States Derived From Noble Gases in Ground Water. Science 256: 1000-1003

Sullivan TM, Pescatore C, 1994. Release of Radon Contaminants from Yucca Mountain: The Role of Buoyancy Driven Flow. Brookhaven National Laboratory BNL-42468.

Sun Y, Carrigan CRCGL (2016) Thermally driven advection for radioxenon transport from an underground nuclear explosion. Geophysical Research Letters 43: 4418-4425

Thomas, J.M., F.C. Benedict, Jr., T.P. Rose, R.L. Hershey, J.B. Paces, Z.E. Peterman, I.M. Farnham, K.H. Johannesson, A.K. Singh, K.J. Stetzenbach, G.B. Hudson, J.M. Kenneally, G.F. Eaton, andD.K. Smith. 2002. Geochemical and Isotopic Interpretations of Groundwater Flow in the Oasis Valley Flow System, Southern Nevada, DOE/NV/11508-56; Publication No. 45190. LasVegas, NV: Desert Research Institute.

Thorstenson, DC, Weeks, EP, Haas H, Busenberg E, Plummer N, Peters, CA, 1998. Chemistry of unsaturated zone gases samples in open boreholes at the crest of Yucca Mountain, Nevada: Data and basic concepts of chemical and physical processes in the mountain. Water Resources Research 34:1507-1529.

742 Tolstikhin, I.N., and I.L. Kamensky. 1969. “Determination of Groundwater Age by the T-3He
743 Method.” In Geochemistry International, Vol. 6: pp. 810–811.

744 Tompson AFB, Bruton CB, Pawloski GA, Smith DK, Bourcier WL, Shumaker DE, Kersting
745 AB, Carle SF, and Maxwell RM (2002), On the Evaluation of Groundwater Contamination from
746 Underground Nuclear Tests, Environmental Geology, 42, 235-247

747 U.S. Department of Energy Environmental Management Nevada Program. 2018. Rainier
748 Mesa/Shoshone Mountain Flow and Transport Model Report Nevada National Security Site,
749 Nevada, Rev. 1. DOE/NV-1588, Las Vegas, Nevada.

750 U.S. Department of Energy Environmental Management Nevada Program. 2019. Record of
751 Technical Change to Nevada National Security Site Integrated Groundwater Sampling Plan, Rev.
752 1, DOE/NV--1525-REV. 1; ROTC No. DOE/NV--1525-REV.1-ROTC 1, 5 February.
753 LasVegas,NV.

754 U.S. Department of Energy Environmental Management Nevada Program. 2020. Written
755 communication. Subject: Pahute Mesa-Oasis Valley Hydrostratigraphic Framework Model for
756 Corrective Action Units 101 and 102: Central and Western Pahute Mesa, Nye County Nevada.
757 September. Las Vegas, NV.

758 US Department of Energy, National Nuclear Security Administration Nevada Field Office 2015
759 United States Nuclear Tests, July 1945 through September 1992, DOE/NV--209-REV 16 Las
760 Vegas, NV

761 Visser, A., D. Hillegonds, and B.K. Esser. 2013a. “Collection and Analysis of Groundwater for
762 Determination of Noble Gas Abundance and Helium Isotopic Composition,” SOP-NGMS-122
763 Revision 5; LLNL-TM-623335. Livermore, CA: Lawrence Livermore National Laboratory,
764 Chemical Services Division.

765 Visser, A., D. Hillegonds, and B.K. Esser. 2013b. “Collection and Analysis of Groundwater for
766 Determination of Tritium by Helium-3 Accumulation,” SOP-NGMS-121 Revision 5; LLNL-
767 TM-623415. Livermore, CA: Lawrence Livermore National Laboratory, Chemical Services
768 Division.

769 Visser A, Moran JE, Hillegonds D, Singleton MJ, Kulongoski JT, Belitz K, Esser BK (2016)
770 Geostatistical analysis of tritium, groundwater age and other noble gas derived parameters in
771 California. Water Research 91: 314-330

772 Visser A, Moran JE, Singleton MJ, Esser BK (2018) Importance of river water recharge to the
773 San Joaquin Valley groundwater system. Hydrological Processes 32: 1202-1213

774 Visser A, Schaap JD, Broers HP, Bierkens MFP (2009) Degassing of 3H/3He, CFCs and SF6 by
775 denitrification: measurements and two-phase transport simulations. Journal of Contaminant
776 Hydrology 103: 206-218

777 Warrier, Rohit B., Maria Clara Castro, and Chris M. Hall (2012) Recharge and source-water
778 insights from the Galapagos Islands using noble gases and stable isotopes. Water Resour. Res. 48
779 (3):W03508.

White, A.F., and N.J. Chuma. 1987. “Carbon and Isotopic Mass Balance Models of Oasis Valley–Fortymile Canyon Groundwater Basin, Southern Nevada.” In Water Resources Research, Vol.23(4): pp. 571–582. Washington, DC: American Geophysical Union.

Winograd IJ, Thordarson W (1975) Hydrogeologic and hydrochemical framework, south-central Great Basin, Nevada-California, with special reference to the Nevada Test Site. USGS Professional Paper 712- C, 134 p.

Winograd IJ, Riggs AC (1984) Recharge to the Spring Mountains, Nevada: isotopic evidence. Geological Society of America Abstracts with Programs 16:698

Winograd IJ, Riggs AC, Coplen TB (1998) The relative contributions of summer and cool-season precipitation to groundwater recharge, Spring Mountains, Nevada, USA. Hydrogeology Journal 6:77-93

Table 1. Noble gas sampling location and area, water levels, recharge/re-equilibration temperatures, terrigenic He, stable isotopes, recharge temperature group, and interpretation.

Location Identifier	Area[a]	Water Level [m asl]	NGRT [°C]	Excess Air, ΔNe [%]	$^4He_{ter}$ / $^4He_{eq}$ [-]	R_{ter}/R_A [-]	$\delta^{18}O$ [‰]	δ^2H [‰]	Group	Interpretation
ER-12-3_m1	RM	1317	16.2	67	21.9	0.01	-14.2	-106.6	B	Pleistocene recharge (Scenario 1)
ER-12-4_m1	RM	1306	20.8	12	1.0	0.08	-13.8	-101.2	C	Local recharge (Scenario 2)
UE-19c WW_m1	PM	1429	12.4	-15	7.6	-	-15.0	-111.0	A	Pleistocene recharge (Scenario 1)
ER-20-6-2_p1	PM	1355	12.6	171	1.6	-	-15.0	-113.0	A	Pleistocene recharge (Scenario 1)
ER-20-6-3_p1	PM	1355	12.1	212	3.0	0.03	-15.0	-113.0	A	Pleistocene recharge (Scenario 1)
U-20 WW_m1	PM	1344	21.5	0*	3.5	0.11	-14.7	-113.0	C	Mixed (Scenario 4)

U-20n PS 1D_o3Z	PM	1344	10.5	36	8.3	55468	-14.6	-112.4	A	Pleistocene recharge (Scenario 1)
ER-20-5-3_m1	PM	1286	14.7	87	5.1	426	-15.2	-114.5	B	Mixed (Scenario 4)
ER-EC-11_m1-2	EC	1273	22.0	15	19.3	0.52	-14.8	-114.3	C	Re-equilibration (Scenario 3) or mixed (Scenario 4)
ER-EC-6_m1-4	EC	1272	19.6	62	15.0	0.70	-15.0	-116.0	C	Re-equilibration (Scenario 3) or mixed (Scenario 4)
ER-EC-12_m1	EC	1270	14.6	162	0.7	0.01	-11.9	-95.9	B	Local recharge (Scenario 2) or mixed (Scenario 4)
ER-EC-12_m2	EC	1270	21.4	37	16.3	0.84	-15.1	-112.9	C	Re-equilibration (Scenario 3) or mixed (Scenario 4)
ER-EC-1_m1-3	EC	1269	20.3	89	6.8	0.62	-14.8	-116.0	C	Re-equilibration (Scenario 3) or mixed (Scenario 4)
ER-EC-15_m1	EC	1267	15.4	125	128.2	0.93	-14.9	-115.7	B	Mixed (Scenario 4)

ER-EC-15_m2	EC	1267	13.9	190	21.7	0.91	-14.7	-116.6	B	Mixed (Scenario 4)
ER-EC-15_m3	EC	1267	26.0	61	39.7	0.96	-14.8	-116.2	D	Re-equilibration (Scenario 3) (geothermal) b or mixed (Scenario 4)
ER-EC-13_m1	EC	1266	31.5	8	6.5	0.84	-14.8	-114.8	E	Re-equilibration (Scenario 3)
ER-EC-13_m2	EC	1266	27.3	78	10.0	0.88	-15.2	-115.7	D	Re-equilibration (Scenario 3) or Mixed (Scenario 4)
ER-EC-14_m1	EC	1263	33.8	38	3.9	1.08	-14.4	-115.3	E	Re-equilibration (Scenario 3) or mixed (Scenario 4)
ER-EC-14_m2	EC	1263	32.3	35	4.1	1.08	-14.3	-115.1	E	Re-equilibration (Scenario 3) or mixed (Scenario 4)
ER-EC-2A_m3	EC	1263	31.3	-3	4.5	0.92	-14.9	-116.0	E	Re-equilibration (Scenario 3)

ER-EC-5_m1-3	EC	1236	30.7	32	4.5	1.10	-14.9	-113.0	E	Re-equilibration (Scenario 3) or mixed (Scenario 4)
ER-EC-7_m1-2	EC	1236	21.7	28	4.3	0.77	-13.2	-98.0	C	Local recharge (Scenario 2)
ER-EC-4_m2-3	EC	1221	32.1	73	11.7	1.02	-14.6	-115.0	E	Re-equilibration (Scenario 3) or mixed (Scenario 4)
ER-EC-8_m1-3	EC	1221	40.7	17	1.7	0.39	-14.8	-116.0	E	Re-equilibration (Scenario 3) or mixed (Scenario 4)
229 S11 E48 01 1 Beatty Wash Windmill Well_s1Q	OV	1250	24.0	0*	14.3	0.84	-12.8	-103.8	C	Local recharge (Scenario 2) or re-equilibration (Scenario 4)
ER-OV-01_p1	OV	1234	28.2	0*	10.5	1.13	-14.7	-112.5	D	Re-equilibration (Scenario 3) or mixed (Scenario 4)
ER-OV-06a_p1	OV	1234	25.3	0*	10.5	1.16	-14.7	-113.0	D	Re-equilibration (Scenario 3) or mixed (Scenario 4)

ER-OV-03c_p1	OV	1211	26.3	20.1*	3.0	0.83	-14.7	-109.0	D	Re-equilibration (Scenario 3) (geothermal) b or mixed (Scenario 4)
Tolicha Peak_o1	OV	1203	16.3	21*	4.2	0.01	-13.5	-103.5	B	Local recharge (Scenario 2)
ER-OV-05	OV	1189	23.6	0*	-	-	-13.7	-106.0	C	Local recharge (Scenario 2) or mixed (Scenario 4)
ER-OV-02_p1	OV	1173	23.6	0*	4.7	1.61	-14.7	-112.0	C	Re-equilibration (Scenario 3) or mixed (Scenario 4)
ER-OV-03a_p1	OV	1152	21.7	38.4*	0.9	1.25	-14.7	-111.0	C	Re-equilibration (Scenario 3) or mixed (Scenario 4)
Goss Springs_g	OV	1150	24.5	104.9*	0.0	-	-14.7	-110.0	D	Re-equilibration (Scenario 3) (geothermal) b or mixed (Scenario 4)
Spdale Upper Well_m1	OV	1142	21.3	0*	5.4	1.11	-13.9	-104.0	C	Local recharge (Scenario 2) or re-

										equilibration (Scenario 4)
Hot Springs Bath House 1_s1	OV	1100	29.2	0*	11.4	1.79	-14.5	-109.0	D	Re-equilibration (Scenario 3) (geothermal) b
ER-OV-04A_p1	OV	1055	22.7	12.7*	2.3	0.82	-14.8	-109.5	C	Re-equilibration (Scenario 3)
ER-18-2_m1	other	1287	63.6	-4	173.7	2.01	-14.7	-110.8	E	Re-equilibration (Scenario 4) (geothermal)
ER-30-1_m1	other	1245	22.6	20	0.5	0.06	-12.0	-90.0	C	Local recharge (Scenario 2)
UE-29a 2_p1	other	1110	19.0	6.7*	0.0	-	-12.7	-92.5	C	Local recharge (Scenario 2)
J-13 WW_m2	other	907	25.3	4	2.8	-	-12.5	-96.0	D	Local recharge (Scenario 2)
J-12 WW_m1	other	853	23.8	3	0.8	-	-13.0	-97.4	C	Local recharge (Scenario 2)

[a] EC = Thirsty Canyon (ER-EC well); FMW = Fortymile Canyon; PM = Pahute Mesa; OV = Oasis Valley; RM = Rainier Mesa

asl: above sea level; NGRT: noble gas recharge/re-equilibration temperature; $^4He_{ter}/^4He_{eq}$: terrigenic He, divided by the equilibrium dissolved He component; R_{ter}/R_A: terrigenic He isotopic ratio (R_{ter}) divided by the atmospheric He isotopic ratio (R_A)

[b] Geothermal refers to samples with noble gas temperatures that are warmer than can be expected from re-equilibration at the regional water-table temperature (Hot Springs, Goss Springs, ER-OV-3c), with unusually high noble gas temperatures (ER-18-2), or with an unusually high measured temperature at the water table (ER-EC-15).

*Excess air ΔNe value derived from unfractionated excess air (UA) noble gas model.

FIGURES:

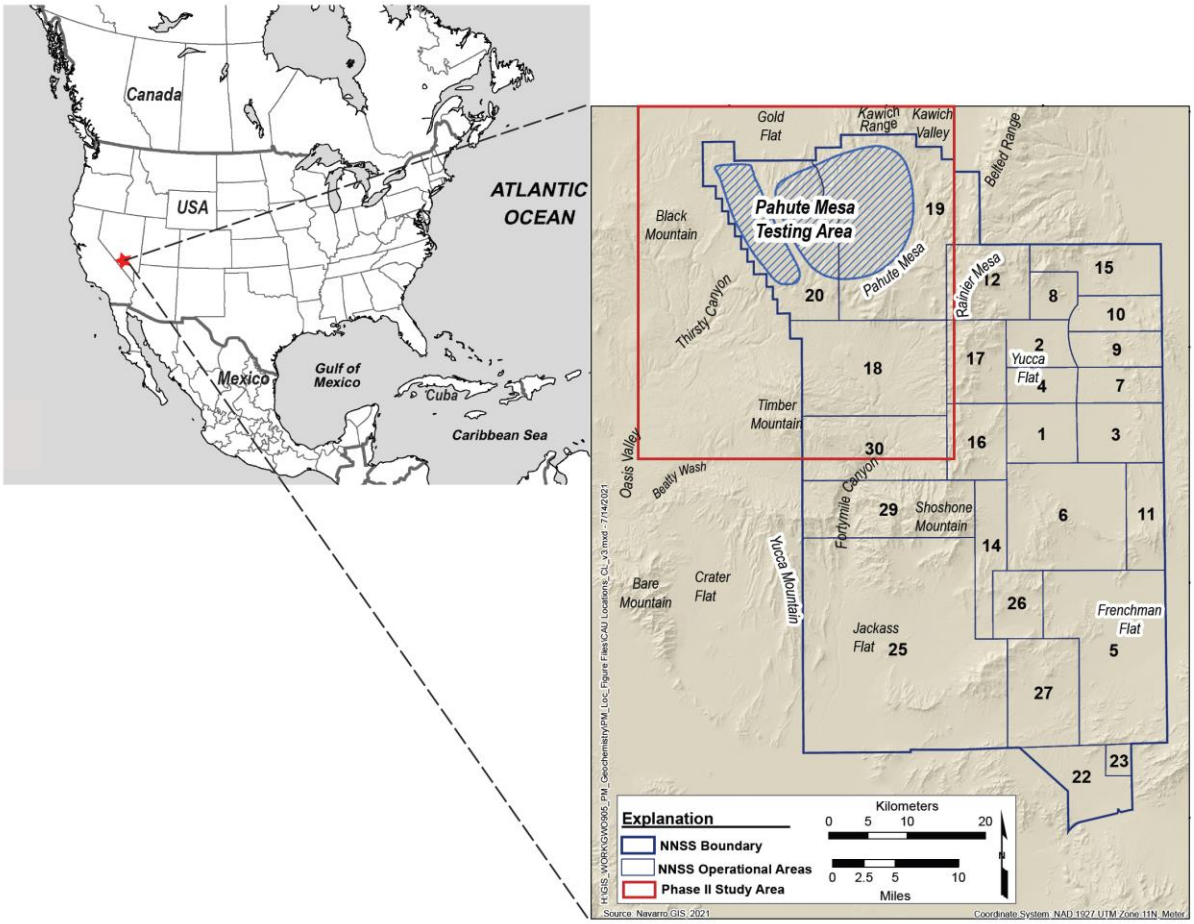

Figure. 1 Nevada National Security Site (NNSS) location with named geographic areas.

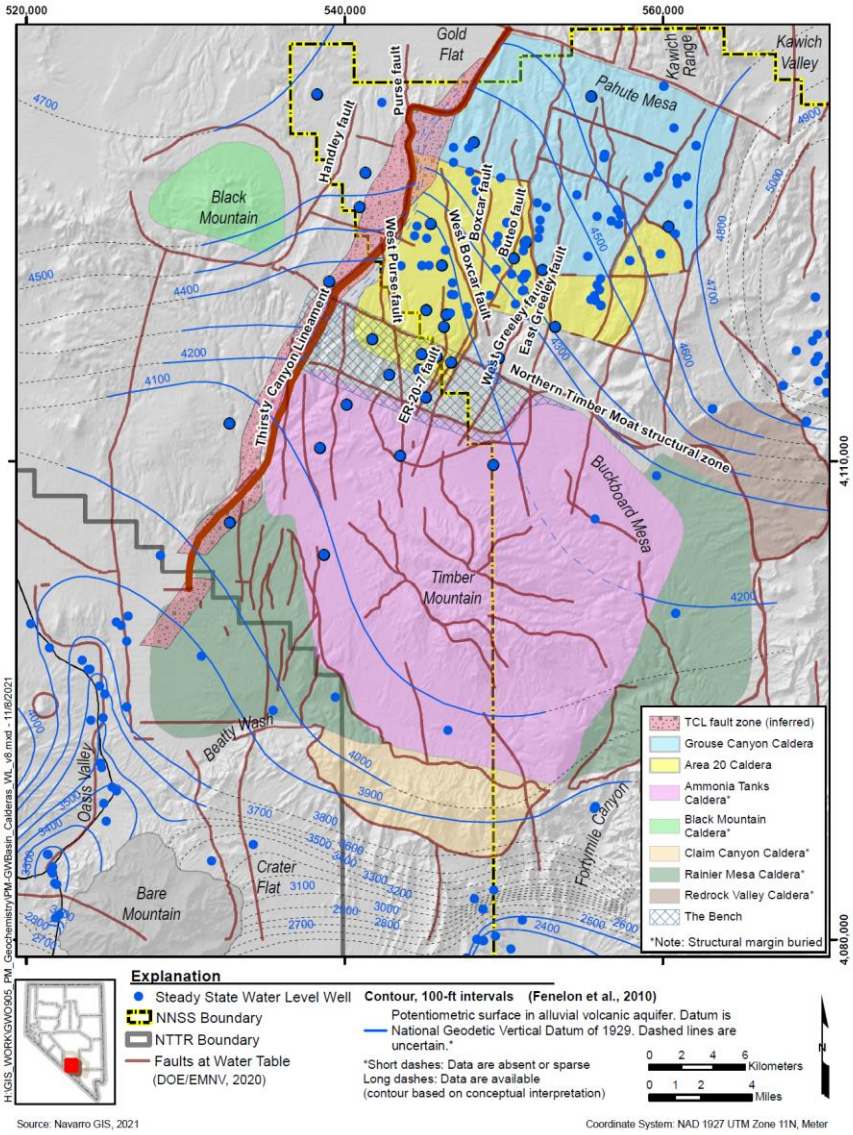

Figure 2. Major structural features, extent of calderas, and water-table contours in the Pahute Mesa area. The Silent Canyon Caldera Complex consists of the Area 20 and Grouse Canyon calderas. The Timber Mountain Caldera Complex (TMCC) consists of the Rainier Mesa and Ammonia Tanks calderas.

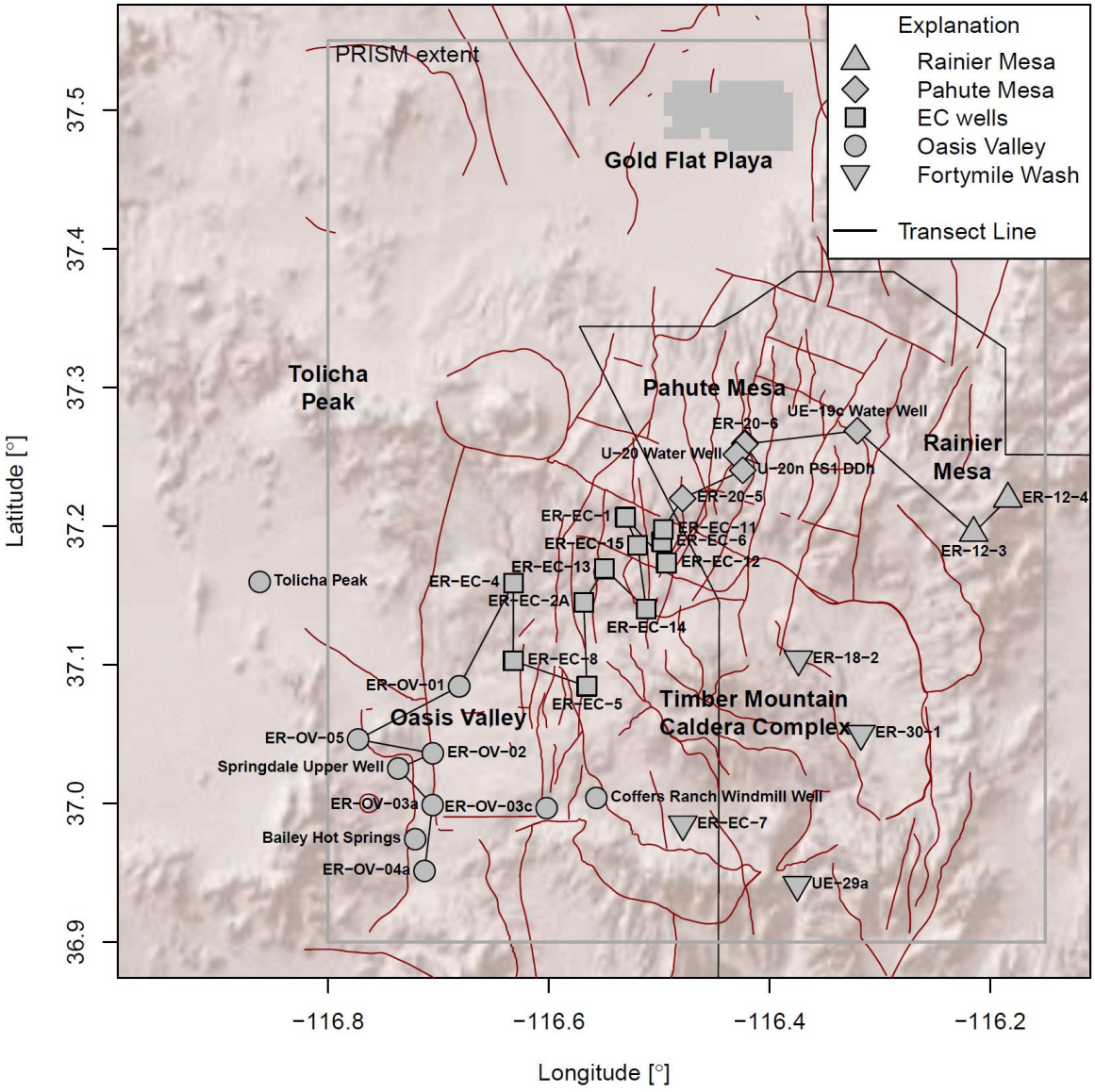

Fig. 3. Locations of wells with noble gas analyses, faults at the water table (dark red lines), the NNSS boundary (black line), Gold Flat playa (grey area), and the spatial extent of the PRISM air temperature analysis (grey box).

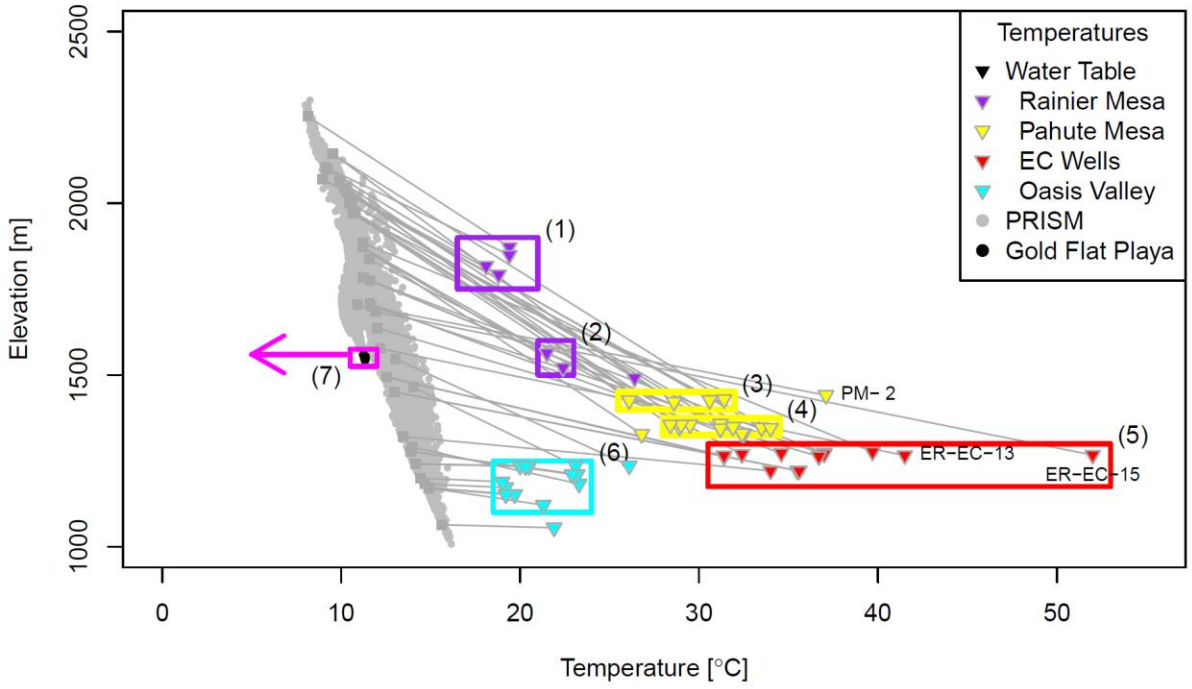

Fig. 4. Mean annual air temperatures (gray dots) from PRISM data show a close correlation with elevation because of the atmospheric lapse rate. The groundwater temperature in the top 1.5 m below the water table is more variable, because of deep water tables and a geothermal gradient of 33 °C per kilometer. Numbered colored boxes indicate potential recharge or re-equilibration conditions for different areas as discussed in the text.

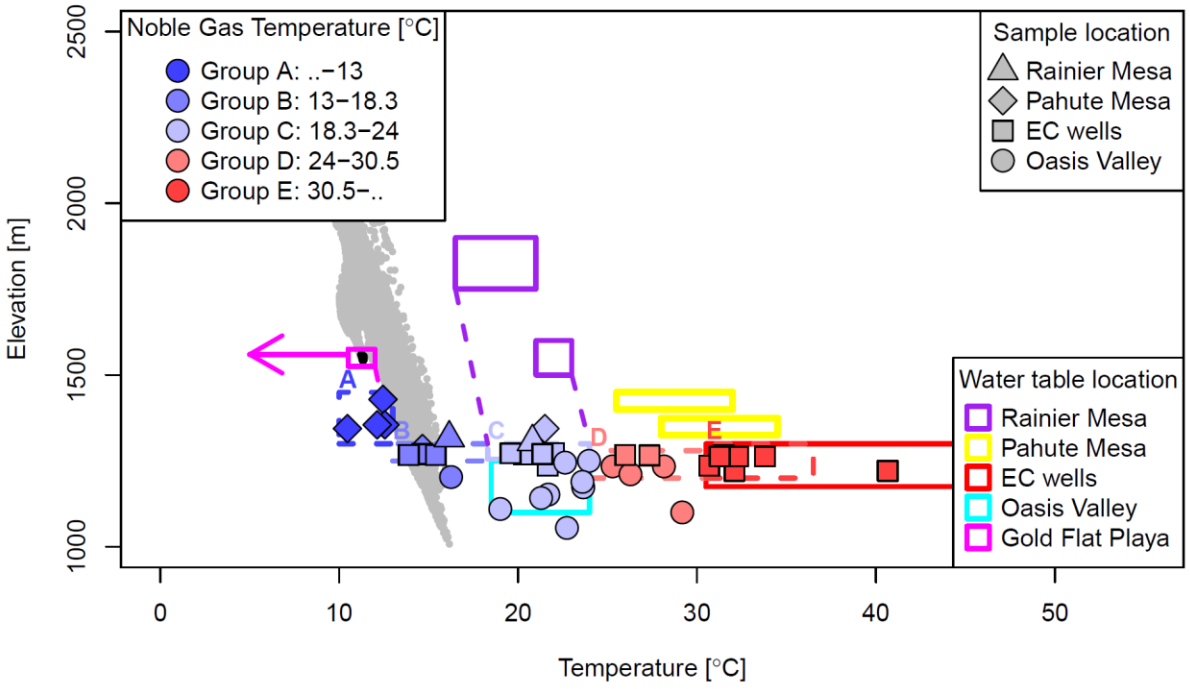

Fig. 5. Noble gas recharge or re-equilibration temperatures (NGRT) plotted at the present-day water-table elevation. Note: Colors indicate NGRT, symbols indicate sample location. Colored boxes indicate potential present-day recharge or re-equilibration conditions.

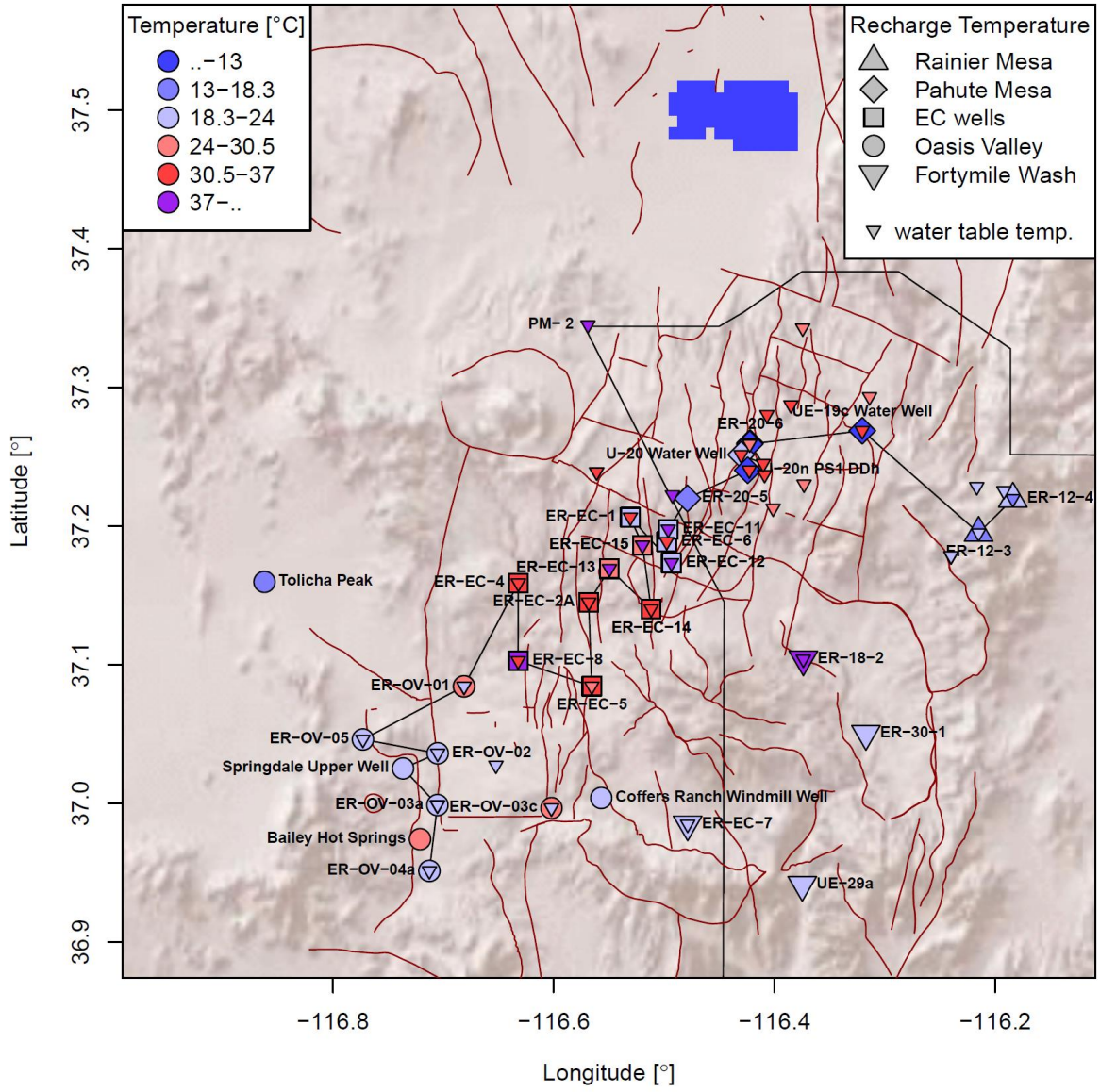

Fig. 6. Map of noble gas recharge/re-equilibration temperatures (large symbols) and groundwater temperatures (small, downward triangles). Note: Blue color of Gold Flat playa reflects present-day mean annual air temperature. Dark red lines indicate the major faults associated with the different caldera complexes.

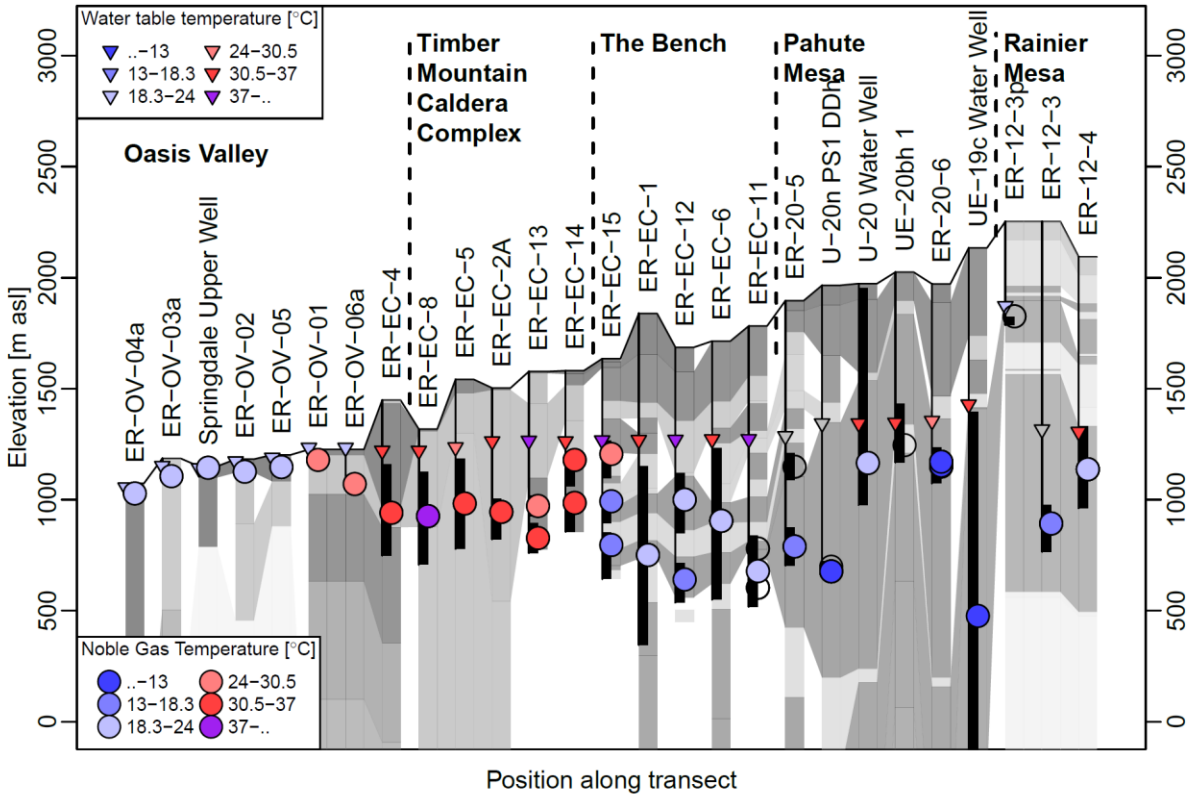

Fig. 7. Cross Section of noble gas recharge/re-equilibration temperatures (large symbols) and groundwater temperatures 1.5 m below the water table (small, downward triangles). Shaded areas indicate connected hydrostratigraphic units (HSU). Black vertical lines indicate the screened interval of the sampled wells.

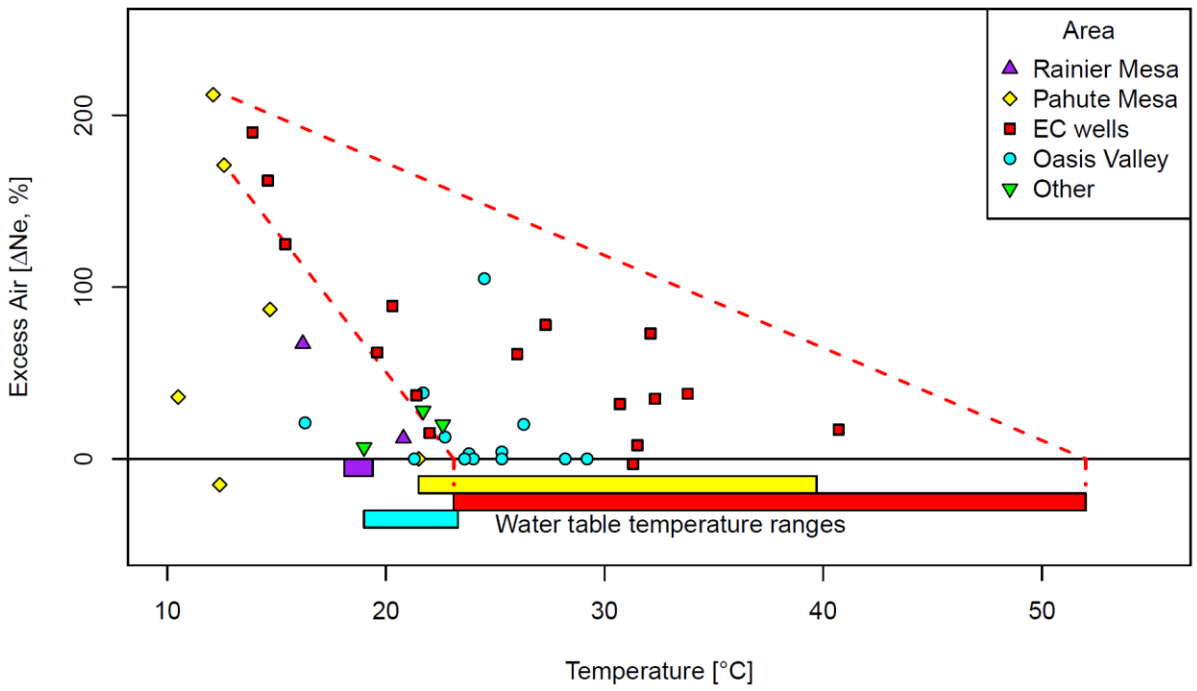

Fig. 8. Excess air (expressed as ΔNe, %) plotted against noble gas temperatures (NGRT, symbols), compared with water table temperature ranges in each of the five areas of the PM-OV groundwater flow system. Dashed red lines indicate the mixing envelop between undisturbed Pahute Mesa groundwater component (low NGRT and high ΔNe) and re-equilibrated groundwater (ΔNe=0, high NGRT) for the range of water table temperatures observed in Thirsty Canyon (EC wells).

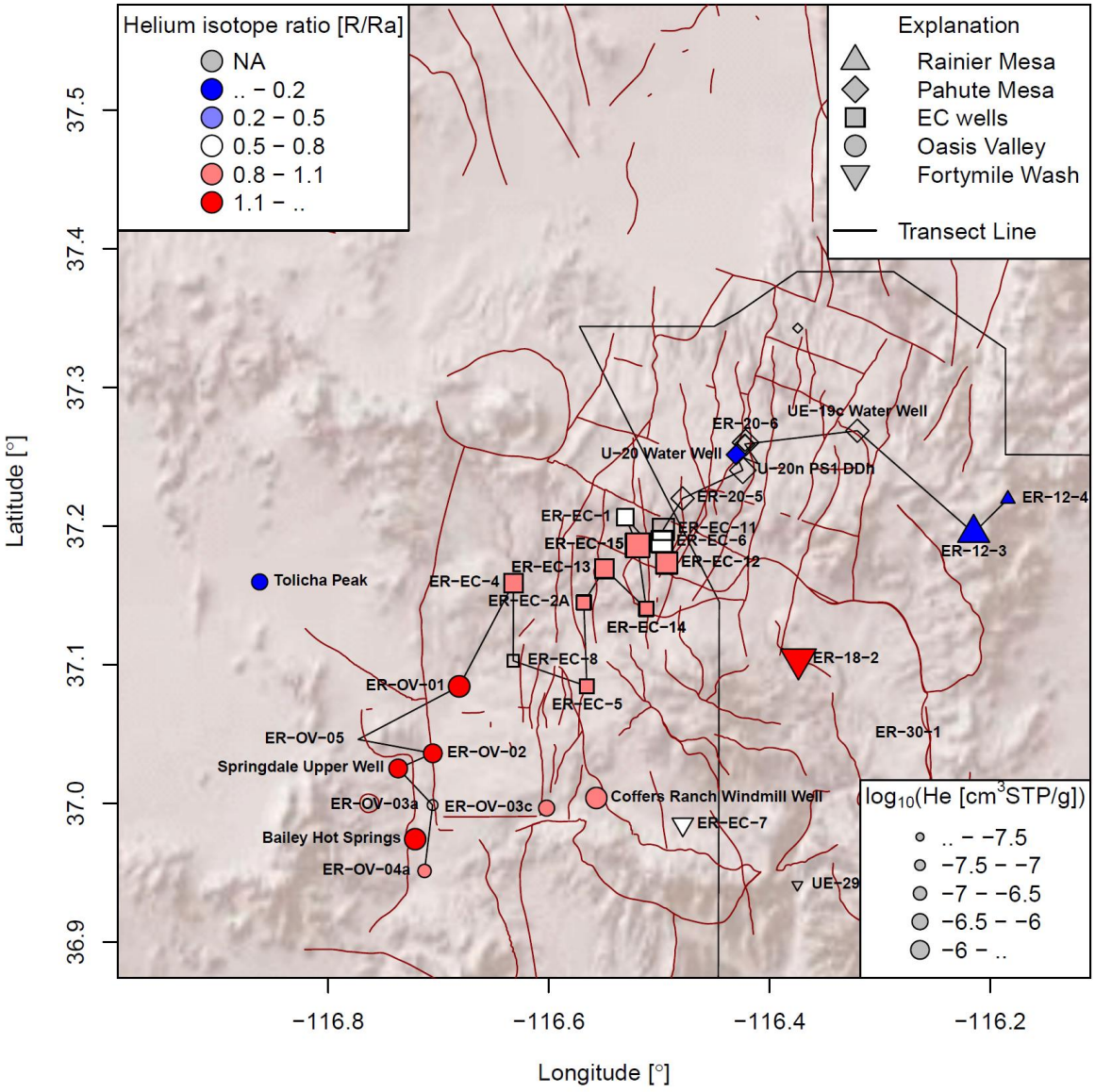

Fig. 9. Map of terrigenic He concentrations and isotopic ratios (R_{ter}) relative to the atmospheric ratio (R_A).

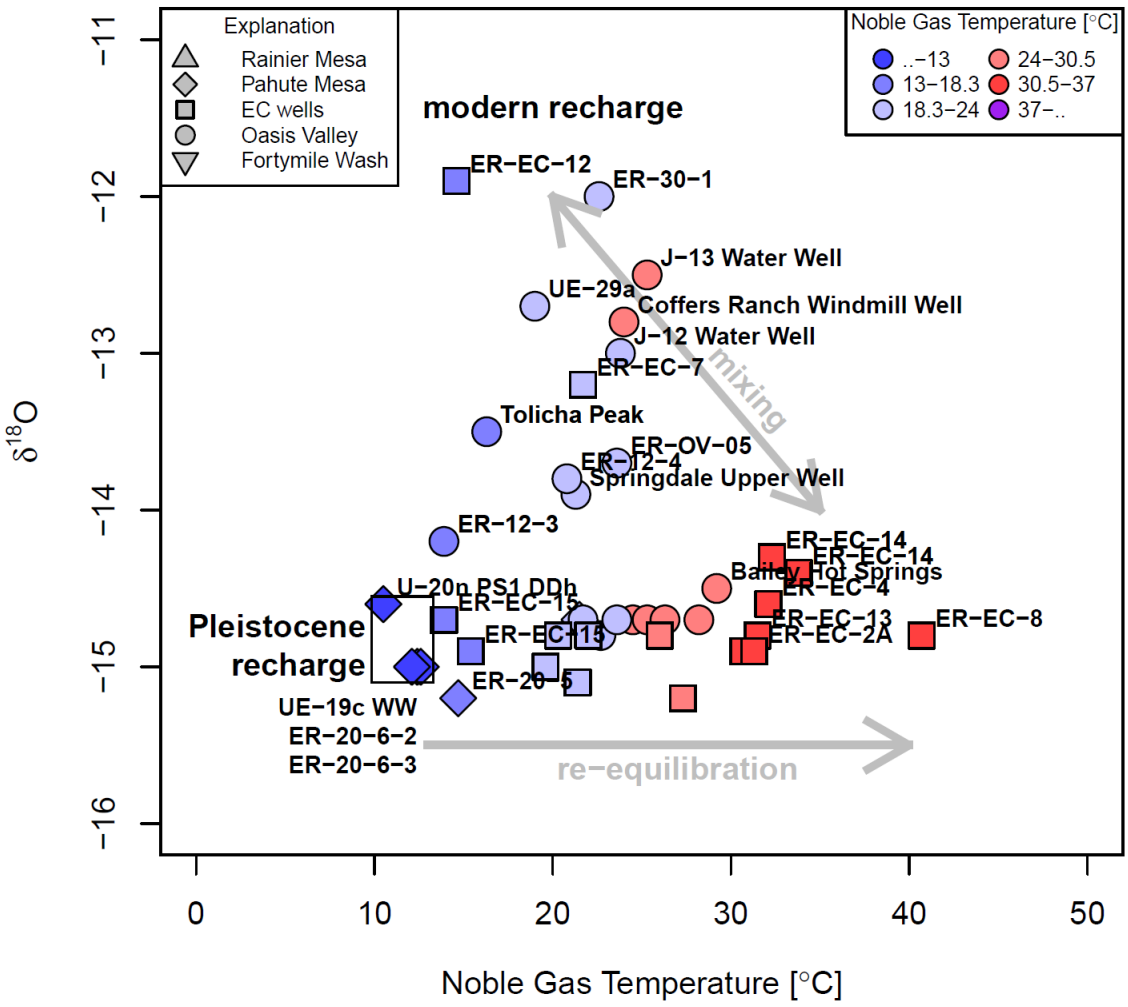

Fig. 10. $\delta^{18}O$ plotted against noble gas recharge/re-equilibration temperature (NGRT) for samples collected from Rainier Mesa, Pahute Mesa, Thirsty Canyon EC-Wells, and Oasis Valley.

Groundwater noble gas measurements confirm paleorecharge hypotheses at Pahute Mesa, Nevada National Security Site, Nevada, USA

Ate Visser,* Edward Kwicklis, Irene Farnham, Andrew F.B. Tompson, and Ronald L. Hershey

*: Corresponding author: visser3@llnl.gov

Supplementary Information 1: Description of the LLNL Noble Gas Mass Spectrometry (NGMS) facility.

The Noble Gas Mass Spectrometer facility at LLNL has been operational for over ten years and has been briefly described in previous publications.(Cey, et al., 2008, Rademacher, et al., 2001) A groundwater sample for analysis of dissolved noble gases is collected by pumping water through a soft copper tube (0.95 cm diameter, 35 cm length) that is subsequently sealed under back-pressure with steel pinch clamps to create a gas-tight cold weld. The cold-welded copper tube typically contains 9.75 grams of water, determined accurately by weighing tube and clamps before and after analysis. The He isotope ratio and abundances of all noble gases (He, Ne, Ar, Kr, and Xe) are measured in groundwater samples in the laboratory by mass spectrometry techniques. The gas samples are prepared for mass spectrometric analysis using a combination of chemical gettering and cryogenic separations.

In the laboratory, each sample tube is attached via a Swagelok fitting to a 250 mL receiving bottle assembly that is part of a 9-port gas-handling manifold (Figure S1: MAN A). (Manifold B is used for tritium samples after ^{3}He accumulation (MAN B).) The sample and receiving volumes (not shown) are evacuated and checked for leaks. The leak checking procedure consists of isolating the sample volume for 30 minutes and then measuring the pressure upon expansion into a portion of the sample-handling manifold. Pressures below 1 x 10^{-5} Torr as measured with a capacitive manometer indicate leak-tight conditions. The water samples contained in the copper sampling tubes are released by removing the bottom clamp. The tubes and receiving volumes are then heated with a heat gun to boil the water and to quantitatively release dissolved noble gases into the headspace. The sample is then frozen to -78 ˚C using dry ice to trap water, and gases are released from the receiving volume into the sample processing manifold.

The released sample gas is expanded into the sample processing manifold along with an isotope dilution spike (SPIKE) consisting of ^{22}Ne, ^{86}Kr and ^{136}Xe. Reactive gases are removed with a titanium-aluminum getter (SAES) operated at 400°C. Ar, Kr and Xe are collected on activated charcoal (AC-CT) at -196˚ C using liquid nitrogen (LN). At this point, a small portion (5%) of the remaining gas phase (He and Ne) is analyzed using a quadrupole mass spectrometer (RGA-200, SRS, Sunnyvale, CA, USA) in order to measure the He/Ne ratio and to determine whether excessive He is present in the sample. If no excessive He is present, all of the remaining He and Ne is collected on activated charcoal (He-CF) at -263º C (10 K) using a mechanical cryogenic cold trap (Janis Research Company, Wilmington, MA, USA). If excessive He is present, the sample is “back expanded” and only a fraction of the sample (1/22.1) is collected on the cold trap. The low-temperature Janis Research charcoal trap is then warmed to -238 °C (35 K) and the

He is released and admitted to the VG5400 mass spectrometer (Isotopx Ltd, Middlewich, Cheshire, UK) for isotopic analysis.

The VG5400 is operated in static mode; the gas sample is expanded into the mass spectrometer vacuum jacket (containing the ion source and detectors) with no vacuum pumps open. The sample is held “statically” within this volume during analysis, as opposed to be continuously leaked into the system while being continuously being evacuated. The static mode is suitable for the chemically inert noble gases and results in a significant increase in sensitivity. The VG5400 uses an electron ionization source (IS) for ion production; a magnetic sector for ion separation with a mass resolving power sufficient to completely resolve ^{3}He atomic ions from $^{1}H^{2}H$ and $^{1}H_{3}$molecular ions. The mass spectrometer uses a conventional 17-stage electron multiplier (EM) and a SR400 pulse counting system (SRS, Sunnyvale, CA, USA) for measuring ^{3}He. Helium-4 is measured using a Faraday Cup (FC) with a 10^{11}-ohm feedback resistor.

The Ar, Kr and Xe collected on the activated charcoal LN trap are desorbed at 150 °C. The Kr and Xe are subsequently sorbed onto a stainless steel cold trap (SS-CT) using LN at -196 °C. Ar pressure is measured using a high sensitivity capacitive manometer and pumped out. The remaining Kr and Xe collected on the stainless steel LN trap are desorbed at room temperature and are measured with the quadrupole mass spectrometer.

The primary calibration standards for dissolved noble gas measurements are air and water containing noble gases in equilibrium with air. Four air standards are analyzed by introducing air into the sample manifold using a pipette system consisting of a 4 L bottle filled with a mixture of

air and known quantities of argon, krypton and xenon (AIR) connected to the manifold via a $0.2cm^3$ aliquot volume. For each aliquot taken, the air reservoir is depleted by 0.005%. The number of aliquots removed is tracked by the computer control system and recorded in a computer file. Manifold blank measurements are made by not opening any of the ports to a sample or standard. The average reproducibility of the air standard within each run is listed in Table S1.

Water standards are prepared by equilibrating tap deionized water with air at a known temperature (approximately room temperature, 25° C) and atmospheric pressure. The equilibration takes place in thermally insulated reservoir filled with about 25 L of water; the large volume allows for stable temperature during equilibration.

The duplicate precision of the instrument (including the sampling procedure) was calculated from 45 duplicates measured between 2010 and 2013, collected by USGS staff under the Priority Basin Program (Belitz, et al., 2003). The reported uncertainty is 2% for $^3He/^4He$, ^4He, Ne and Ar, and 3% for Kr and Xe.

Table S1: Characteristics of the traditional LLNL Noble Gas Mass Spectrometry (NGMS) system

	$^{3}He/^{4}He$	^{4}He	Ne	Ar	Kr	Xe
Measurement	VG5400	VG5400	SRS RGA200	Capacitance manometer	SRS RGA200	SRS RGA200
Air standard reproducibility	1.5%	0.5%	1.4%	0.1%	1.5%	2.0%
Sample duplicate precision	2.6%	4.7%	6.4%	2.5%	1.7%	3.0%
Reported instrument uncertainty	2%	2%	2%	2%	3%	3%

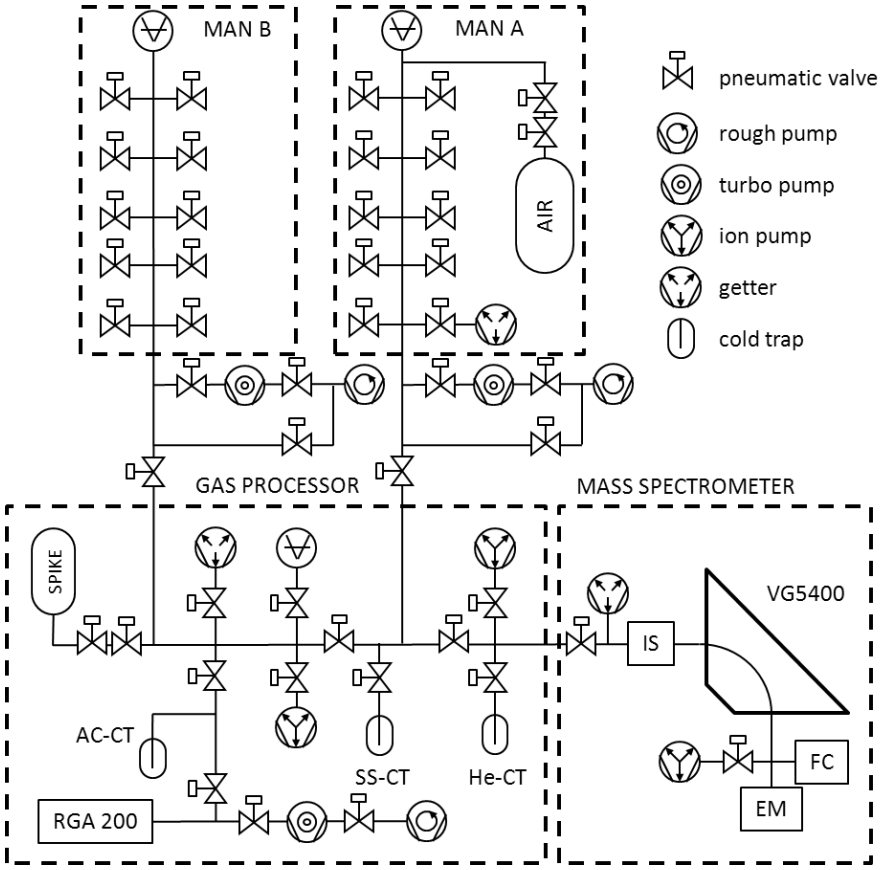

Figure S1: Schematic of the LLNL Noble Gas Mass Spectrometry (NGMS) system.

Supplementary Information 2: Quality Control of Noble Gas Data

The Noble Gas Mass Spectrometer Facility at LLNL has been operational since 1993. During that time, nearly 200 noble gas analyses have been performed on groundwater samples from the NNSS. These data have been compiled, verified, and reported in a digital format. The sample collection and analysis protocols are described in detail in standard operating procedures (Visser et al., 2013a and b). All uploaded analyses meet minimum data quality objectives and quality assurance /quality control (QA/QC) as outlined in these standard operating procedures.

Noble gases in groundwater are predominantly from atmospheric origin. The composition of dissolved noble gases from atmospheric origin is controlled by the noble gas abundances in the atmosphere, air pressure (recharge altitude), and temperature dependent solubility. The differences in noble gas solubility result in specific, temperature-dependent noble gas concentration ratios. Water-table fluctuations cause air entrapment in the unsaturated zone, leading to excess dissolution of noble gases with an atmospheric abundance signature. As a result of these processes, the concentrations of noble gases are constrained and consistent with one another.

Besides an atmospheric origin, He isotopes (^{3}He and ^{4}He) in groundwater can be derived from nuclear fission of lithium-6 (^{6}Li) (nucleogenic ^{3}He); production of ^{4}He by uranium (U)-thorium (Th) decay (radiogenic ^{4}He); mantle He (^{3}He and ^{4}He); and ^{3}H decay (tritiogenic ^{3}He) (Tolstikhin and Kamensky, 1969). “Terrigenic He” refers to the combined He contribution from nucleogenic, radiogenic, and mantle sources.

The quality of the noble gas data is checked by comparing the measured concentrations with a model that considers the solubility equilibrium concentrations for the given recharge altitude and a fitted recharge temperature, and realistic excess-air amounts. If the measured concentrations of noble gases in the sample are improbable, a duplicate sample is measured.

The data were analyzed for outliers in two ways: (1) outliers within the distribution of the specific noble gas concentrations, and (2) groups of outliers with respect to the concentrations of other noble gases. No outliers in the He isotopic ratio and He concentration were removed because of the skewed distribution of these measurements. Because none of the noble gas concentration distributions are normal, outlier tests based on the normality assumption cannot be performed. Selection criteria for outliers within the noble gas concentration distribution were subjectively formulated. The criterion for high value outliers was that the value was more than the interquartile range larger than the next smaller value. Values above that criterion were considered outliers.

Groups of outliers with respect to the concentrations of other noble gases were derived from visual inspection of figures plotting concentrations of each noble gas against the concentration of all other noble gases. Twenty measurements were removed as outliers as a result of this comparison. The remaining dataset still shows a number of outliers, compared to expected noble gas concentrations, based on the currently accepted models for noble gas dissolution. No further efforts to remove data were made, to avoid constraining the data to currently accepted models. The data will likely contain measured values that are improbable.

For Pahute Mesa, noble gas data from 37 locations (springs, wells, or multilevel wells; Supplementary Table 1 and Fig. 3 in the main article) were included in this paper (Supplementary Table 2). Forty-two analyses from Pahute Mesa were available for interpretation of the noble gas recharge temperature (NGRT) and terrigenic He content. If multiple noble gas analyses (sample replicates or different sampling dates) were available for the same well/screen, a single analysis was selected for interpretation. The selection was based on analytical QA/QC notes, whether analysis for all noble gases was available, and the goodness-of-fit with respect to dissolution models.

Supplementary Information 3: Conceptual Models for Noble Gas Re-equilibration

The noble gas concentrations in Pahute Mesa area groundwater are the consequence of many possible groundwater recharge and flow processes that affect gas-water partitioning, like equilibrium dissolution, excess air formation, re-equilibration, and mixing. The noble gas measurements in this dataset cannot be used precisely identify all processes and associated parameters necessary to formulate exact equations for interpreting noble gas concentrations. Instead, we used a simplified conceptual model to interpret the noble gas concentrations in samples that appear to have been affected by re-equilibration. The simplified model represents three processes:

1. Recharge of Pleistocene groundwater at a temperature of 15 °C with the addition of up to 0.02 cm^3STP/g unfractionated excess air (ΔNe = 213%).
2. Re-equilibration of groundwater at a temperature of 50 °C with a vadose zone gas with atmospheric composition, resulting in a ΔNe value of 0%.
3. Linear mixing between initial and re-equilibrated groundwater.

The resulting dissolved noble gas concentrations for these processes can be calculated as follows:

1. $C_{0,i} = f(T_0, EA) = (k_i(T_0) + EA) \times X_{atm,i}$
2. $C_{R,i} = f(T_R) = k_i(T_R) \times X_{atm,i}$
3. $C_{S,i} = f_{LM} \times C_R + (1\text{-}f_{LM}) \times C_0$

Where C is the concentration of atmospheric noble gas i (Ne, Ar, Kr, Xe), initially (C_0), after re-equilibration (C_R), and in the sample (C_s); T_0 is the initial recharge temperature; $k_i(T)$ is the Henry's law dissolution coefficient at temperature T; EA is the amount of unfractionated excess air entrained during recharge (cm_3STP/g); $X_{atm,i}$ is the atmospheric noble gas concentration; T_R is the re-equilibration temperature; and f_{LM} is the fraction of re-equilibrated groundwater in the sample (C_s). Air pressure is assumed to be 900 mbar, reflecting a water table elevation of 1000 m.

The effect of re-equilibration and linear mixing is illustrated in figure S2. The initial recharge concentrations (C0), containing 0.02 cm^3STP/g excess air, are all above the concentration in equilibrium with the atmosphere at the same temperature (Ceq). Complete re-equilibration results in relative concentrations below Ceq for all noble gases. Linear mixing between the two endmembers (C0 and CR) affect all noble gases proportionally.

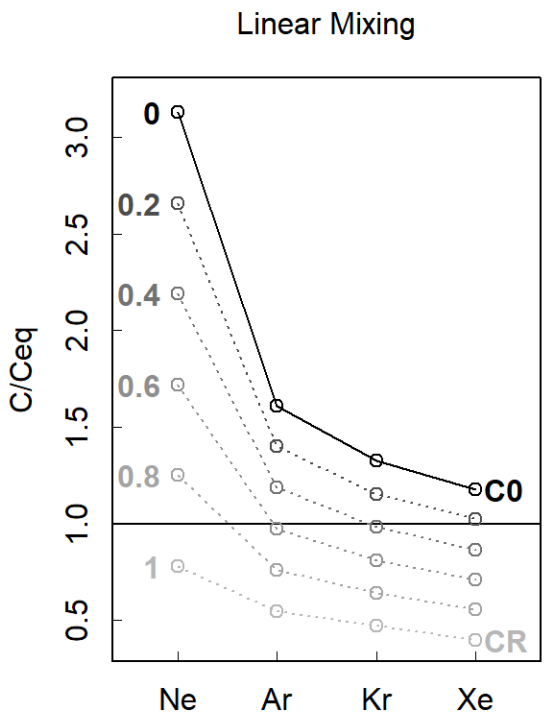

Figure S2: The effect of linear mixing between initial recharge concentrations (C0, T=15 °C, EA=0.02 cm^3STP/g) and concentrations re-equilibrated at T=50 °C (CR), relative to the concentrations in equilibrium with the atmosphere at 15 °C (Ceq).

The four parameters (T_0, EA, T_R, f_R) cannot be derived from a single measurement of four atmospheric concentrations. Instead, we fitted the measured noble gas concentrations to the unfractionated excess air (UA) model constrained by the apparent noble gas (re)equilibration temperature and the apparent excess air component (EA). The reduced number of parameters allowed us to include a larger number of samples (with fewer than four atmospheric nobles gas measurements) and expand the spatial coverage and hydrogeological insights.

The simplified model fit would be a precise estimate of the T and EA parameters if all noble gases responded linearly to both parameters. While EA is a linear addition of atmospheric air to the equilibrium concentration, the temperature-dependence of the Henry's Law dissolution coefficient is non-linear. However, a binary (50%-50%) mixture of an initial recharge at 15 °C and no excess air and a re-equilibration at 50 °C results in an apparent fit with a temperature of 27.7 °C (instead of 32.5 °C) and modeled concentration residuals between -1.8% for neon and +2.1% for xenon. These residuals are negligible considering the range of noble gas concentrations measured in the samples from Pahute Mesa. While the apparent temperature does

not precisely reflect the average of the two temperatures, it provides a reliable indicator of whether a sample has been affected by re-equilibration at a higher temperature.

The simplified model fit is illustrated in Figure S3, showing the dissolved atmospheric noble gas concentrations plotted against one-another. The lines connect the modeled concentrations after recharge at 15 °C with no excess air (Ceq) or with 0.02 cm^3STP/g excess air (C0, ΔNe=213%) and after re-equilibration at 50 °C. The majority of the samples fall within the triangle that describes the range of concentrations expected from the simplified recharge-re-equilibration-mixing conceptual model. The assumed recharge and re-equilibration temperatures, as well as the location of the affected samples, are consistent with the hydrogeological knowledge of the Pahute Mesa area described in detail in Kwicklis et al. (2021).

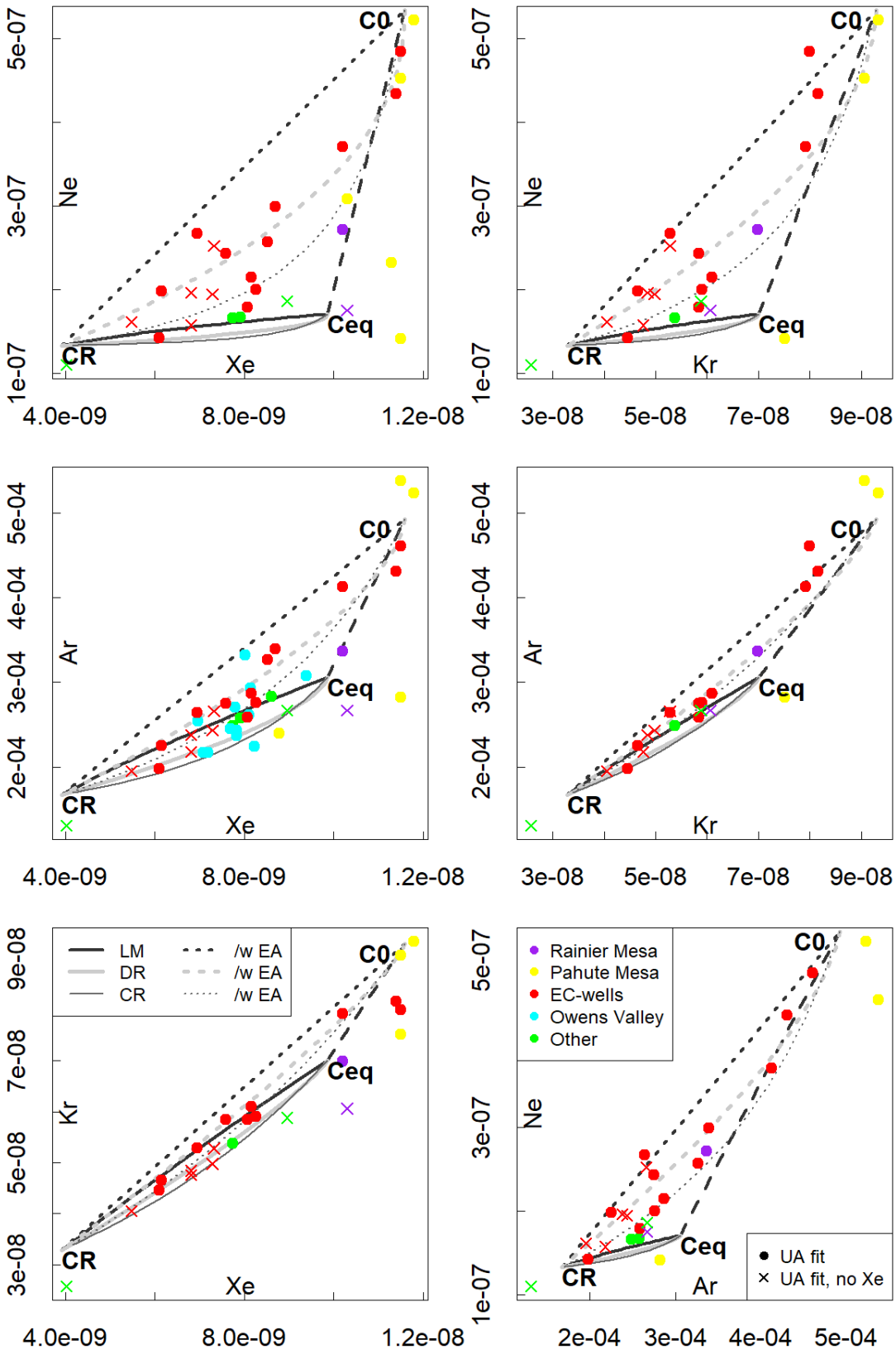
C0
Ceq
CR
Ne
Xe
Kr
Ar
LM
DR
CR
/w EA
/w EA
/w EA
Rainier Mesa
Pahute Mesa
EC-wells
Owens Valley
Other
UA fit
UA fit, no Xe
5e-07
3e-07
1e-07
4.0e-09
8.0e-09
1.2e-08
3e-08
5e-08
7e-08
9e-08
5e-04
4e-04
3e-04
2e-04

Figure S3: Dissolved atmospheric noble gas concentrations plotted against one-another. Colors indicate the sample location. Ceq, C0, and CR are the modeled concentrations at the initial recharge temperature (Ceq, T=15 °C) with excess air (C0, EA=0.02 cm^3STP/g) and the concentrations after re-equilibration at 50 °C. The triangle between Ceq, C0, and CR indicates the range of possible concentrations from recharge, re-equilibration and linear mixing (LM). Additional scenarios (diffusive re-equilibration (DR) and closed-system re-equilibration (CR), discussed in the text) extend the envelope of possible concentrations below the Ceq-CR linear mixing line and encompass nearly all measured concentrations. Concentrations are expressed in cm^3STP/g.

However, the Ar-Xe plot shows a group of 8 samples (plotted with × symbols) that have elevated Xe concentrations with respect to Ar. These samples could only be fitted to the simplified model if the Xe measurement was excluded. Two additional conceptual models to describe re-equilibration could explain this excess Xe: re-equilibration in a closed-system (closed-system re-equilibration, CR) and re-equilibration limited by diffusion (diffusive re-equilibration, DR).

In the first additional conceptual model, re-equilibration occurs with a gas phase that is not in free exchange with the atmosphere. Instead, the noble gases exsolving from groundwater can accumulate in the gas phase above atmospheric concentrations. The concentration of dissolved noble gases after closed-system re-equilibration ($C_{CR,i}$) is given by:

$$C_{CR,i} \times V_w + X_{R,i} \times V_g = C_{0,i} \times V_w + X_{atm,i} \times V_g$$

With V_w the volume of water that re-equilibrates with a volume gas V_g, and $X_{R,i}$ the concentration of noble gas i in the re-equilibrated gas phase. The re-equilibrated dissolved noble gas concentration can then be calculated as:

$$C_{CR,i} = (C_{0,i}+f_g \times X_{atm,i}) / (1+f_g / k_i(T_R))$$

With f_g the gas phase volume expressed as a fraction of the water volume ($f_g = V_g/V_w$). Closed-system re-equilibration leads to apparent enrichment of the more soluble and more temperature sensitive heavier noble gases with respect to the lighter noble gases. This re-equilibration scenario is similar to the closed-system equilibrium (CE) excess air model. (Aeschbach-Hertig, et al., 2000)

In the second additional conceptual model, the degree of re-equilibration is controlled by the diffusivities of the noble gases. The concentration of dissolved noble gases after re-equilibration ($C_{DR,i}$) is given by:

$$C_{DR,i} = C_{0,i} + (C_{R,i} - C_{0,i}) \times f_R^{(DNe/Di)}$$

With $C_{0,i}$ and $C_{R,i}$ the noble gas concentrations initial after recharge and after complete re-equilibration, f_R the progression of re-equilibration of neon (between 0 and 1) and DNe and Di the diffusivities of neon and noble gas i. This re-equilibration scenario is similar to the partial re-equilibration (PR) excess air model. (Stute, et al., 1995)

Both additional conceptual models result in relative enrichment of the heavier noble gases compared to the lighter noble gases (Figure S4), either because of lower diffusivities (Diffusive Re-equilibration, left figures) or higher solubilities and temperature sensitivity (Closed-System Re-equilibration, right figures). If the initial concentrations are in equilibrium with the atmosphere (top figures), i.e., no excess air, the relative concentrations of Kr and Xe are higher than of Ar for partial re-equilibration up to 0.6 or a relative gas volume up to 0.05.

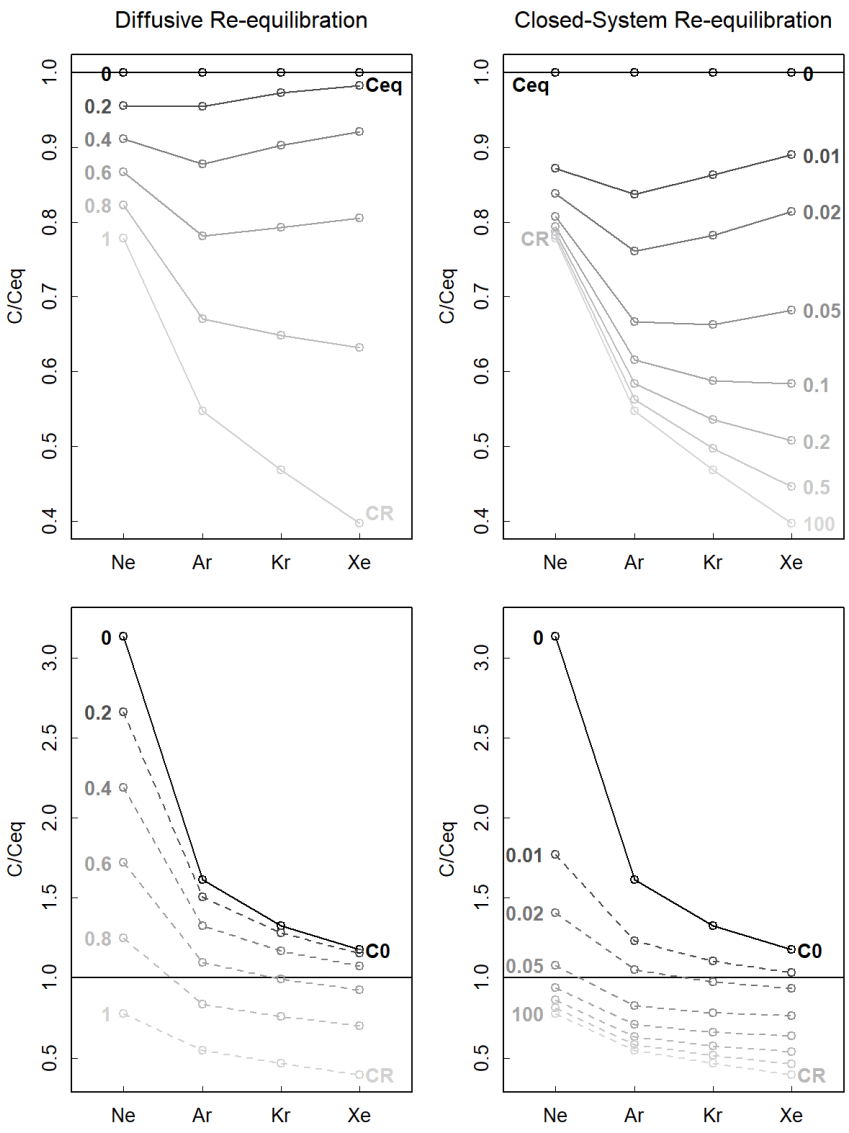

Figure S4: Effects of Diffusive Re-equilibration (left figures) and Closed-System Re-equilibration (right figures) of initial concentrations in equilibrium with the atmosphere (Ceq) or with a 0.02 cm^3STP/g excess air component (C0). Numbers represent the progression of re-equilibration (f_R) in the DR model and the relative gas volume (f_g) in the CR model.

The effect of these conceptual models is also illustrated in Figure S3. The envelope of possible noble gas concentrations extends below the linear mixing between Ceq and CR and encompasses nearly all observed noble gas concentrations.

These additional conceptual models were explored to gain a better understanding of potential noble gas re-equilibration processes. We used the simplified conceptual model to interpret the noble gas concentrations in samples that appear to have been affected by re-equilibration because the four atmospheric noble gases cannot uniquely identify all parameters of these additional conceptual models.

A recent study provided experimental evidence for the adsorption of xenon and argon to zeolitized rhyolitic tuff samples from the NNSS through a series of pure-gas pycnometry measurements. (Feldman, et al., 2020) While no adsorption was observed on non-zeolotized samples, the uptake parameter values for the zeolitized rhyolitic tuff samples for argon (1.8) and xenon (9.8) are much higher than for helium (0.53), equivalent to retardation factors for argon and xenon of 3.41 and 18.28. While this study omitted water from the experiments, previous studies showed that the interaction between adsorbed xenon and water is dependent on the structure of the zeolite (Hu, et al., 2018) and the xenon adsorption sites can be competitively occupied by water molecules prohibiting xenon adsorption. Although adsorption and possible retardation of noble gases at in-situ water saturation conditions is expected to be sensitive to zeolitization, at this time it is unclear to what extent. The retardation is expected to be most pronounced when there is a passing tracer front or when the noble gas (isotope) of interest is radioactive and short-lived.

While adsorption to zeolotized rhyolitic tuffs may play a role in noble gas transport at the NNSS, re-equilibration due to flow barriers or upwelling is the most likely scenario because (1) elevated NGRTs are limited to an area (Timber Mountain Caldera Complex) where they coincide with elevated water table temperatures and high geothermal gradients are observed and (2) re-equilibration coincides with changes in terrigenic helium suggesting the influence of geothermal features.

References

Aeschbach-Hertig W, Peeters F, Beyerle U, Kipfer R (2000) Palaeotemperature reconstruction from noble gases in ground water taking into account equilibration with entrapped air. Nature 405: 1040

Belitz K, Dubrovsky NM, Burow K, Jurgens B, Johnson T (2003) Framework for a Ground-Water Quality Monitoring and Assessment Program for California, Water Resources Investigation Report 03-4166 USGS Water Resources Investigation Report 03-4166, Sacramento, CA, USA.

Cey BD, Hudson GB, Moran JE, Scanlon BR (2008) Impact of Artificial Recharge on Dissolved Noble Gases in Groundwater in California. Environ Sci Technol 42: 1017-1023

Feldman J, Paul M, Xu G, Rademacher DX, Wilson J, Nenoff TM (2020) Effects of natural zeolites on field-scale geologic noble gas transport. Journal of Environmental Radioactivity 220-221: 106279 DOI https://doi.org/10.1016/j.jenvrad.2020.106279

Hu Y, Li M, Hou G, Xu S, Gong K, Liu X, Han X, Pan X, Bao X (2018) The role of water in methane adsorption and diffusion within nanoporous silica investigated by

hyperpolarized 129Xe and 1H PFG NMR spectroscopy. Nano Research 11: 360-369 DOI 10.1007/s12274-017-1638-8

Kwicklis E, Farnham I, Hershey RL, Visser A, Hoaglund J (2021) Understanding long-term groundwater flow at Pahute Mesa and vicinity, Nevada National Security Site, USA, from naturally occurring geochemical and isotopic tracers. Hydrogeology Journal DOI 10.1007/s10040-021-02397-x

Rademacher LK, Clark JF, Hudson GB, Erman DC, Erman NA (2001) Chemical evolution of shallow groundwater as recorded by springs, Sagehen basin; Nevada County, California. Chem Geol 179: 37-51

Stute M, Forster M, Frischkorn H, Serejo A, Clark JF, Schlosser P, Broecker WS, Bonani G (1995) Cooling of Tropical Brazil (5ºC) during the Last Glacial Maximum. Science 269: 379

Hydrogeology Journal - Electronic Supplementary Material (ESM1)

Using groundwater noble gas measurements to confirm paleorecharge hypotheses at Pahute Mesa, Nevada National Security Site, Nevada, USA

Ate Visser,* Edward Kwicklis, Irene Farnham, Andrew F.B. Tompson, and Ronald L. Hershey

*: Corresponding author: visser3@llnl.gov

Supplementary Tables

Table S1 Location and well information
Table S2 Measured noble gas concentrations
Table S3 Derived parameters

Table S1 Location and well information

Location Identifier	Area	Latitude	Longitude	Ground Surface Elevation [m asl]	Top of Well Screen [m asl]	Bottom of Well Screen [m asl]	Water Level [m asl]	Water Table Temperature [C]
ER-12-3_m1	RM	37.195	-116.215	2275	998	788	1317	
ER-12-4_m1	RM	37.2196	-116.184	2101	1339	969	1306	31.5
UE-19c WW_m1	PM	37.2687	-116.3204	2139	1401	-448	1429	31.4
ER-20-6-2_p1	PM	37.2599	-116.4221	1970	1234	1072	1355	29
ER-20-6-3_p1	PM	37.2591	-116.4224	1970	1228	1114	1355	28.4
U-20 WW_m1	PM	37.2514	-116.4302	1983	1963	987	1344	31.2
U-20n PS 1D_o3Z	PM	37.2402	-116.4242	1974	693	661	1344	
ER-20-5-3_m1	PM	37.2199	-116.4788	1896	876	703	1286	
ER-EC-11_m1-2	EC	37.1976	-116.4962	1783	838	518	1273	37
ER-EC-6_m1-4	EC	37.1887	-116.4976	1728	1246	564	1272	34.6
ER-EC-12_m1	EC	37.1734	-116.4933	1701	729	552	1270	37
ER-EC-12_m2	EC	37.1734	-116.4933	1701	1136	865	1270	37
ER-EC-1_m1-3	EC	37.2063	-116.5306	1841	1153	349	1269	32.4
ER-EC-15_m1	EC	37.1861	-116.5195	1684	900	692	1267	52
ER-EC-15_m2	EC	37.1861	-116.5195	1684	1041	944	1267	52
ER-EC-15_m3	EC	37.1861	-116.5195	1684		1145	1267	52
ER-EC-13_m1	EC	37.1692	-116.5495	1577	894	760	1266	41.5
ER-EC-13_m2	EC	37.1692	-116.5495	1577	1018	926	1266	41.5
ER-EC-14_m1	EC	37.1402	-116.5117	1636	1060	911	1263	36.7
ER-EC-14_m2	EC	37.1402	-116.5117	1636	1241	1117	1263	36.7
ER-EC-2A_m3	EC	37.1449	-116.5683	1535	1037	853	1263	31.4
ER-EC-5_m1-3	EC	37.0845	-116.5655	1542	1186	780	1236	26.1

ER-EC-7_m1-2	EC	36.9849	-116.4786	1468	1197	1046	1236	23.1
ER-EC-4_m2-3	EC	37.1588	-116.632	1436	1146	736	1221	35.5
ER-EC-8_m1-3	EC	37.1028	-116.6322	1327	1134	717	1221	34
229 S11 E48 01 1 Beatty Wash Windmill Well_s1Q	OV	37.0039	-116.5569	1367			1250	
ER-OV-01_p1	OV	37.0844	-116.6812	1228	1182	1176	1234	20.5
ER-OV-06a_p1	OV	37.0844	-116.6812	1228	1074	1068	1234	20
ER-OV-03c_p1	OV	36.9966	-116.602	1312	1156	1150	1211	23.2
Tolicha Peak_o1	OV	37.1597	-116.862	1223	3932	612	1203	
ER-OV-05	OV	37.0461	-116.7728	1202	1150	1144	1189	19
ER-OV-02_p1	OV	37.0361	-116.7051	1181	1129	1123	1173	19.2
ER-OV-03a_p1	OV	36.9988	-116.7053	1176	1109	1103	1152	19.7
Goss Springs_g	OV	36.9994	-116.7067	1176			1150	
Spdale Upper Well_m1	OV	37.0252	-116.7365	1146	1146	1146	1142	21.1
Hot Springs Bath House 1_s1	OV	36.9742	-116.7211	1112			1100	
ER-OV-04A_p1	OV	36.9513	-116.7126	1065	1031	1025	1055	21.9
ER-18-2_m1	other	37.1039	-116.3738	1595	1183	833	1287	46.2
ER-30-1_m1	other	37.0502	-116.3171	1426	1220	1185	1245	
UE-29a 2_p1	other	36.9413	-116.3748	1226	1139	804	1110	
J-13 WW_m2	other	36.808	-116.3955	1011		-52	907	
J-12 WW_m1	other	36.7649	-116.391	951		604	853	

Table S2 Measured noble gas concentrations

Location Identifier	date	He3He4	He3He4_unc	He4	He4_unc	Ne	Ne_unc
ER-12-3_m1	5/1/2015	1.16E-07	3.89E-09	9.23E-07	1.84E-08	2.71E-07	5.43E-09
ER-12-4_m1	5/9/2015	7.83E-07	1.76E-08	8.04E-08	1.60E-09	1.75E-07	3.50E-09
UE-19c WW_m1	8/13/1992			3.34E-07		1.41E-07	
ER-20-6-2_p1	11/27/1996			1.83E-07		4.52E-07	
ER-20-6-3_p1	12/16/1996	9.27E-07	1.85E-08	2.60E-07		5.22E-07	
U-20 WW_m1	11/5/1997	4.69E-07	9.38E-09	1.75E-07			
U-20n PS 1D_o3Z	7/9/2003	2.08E-01	4.16E-03	3.79E-07		2.32E-07	
ER-20-5-3_m1	11/15/2001	1.08E-03	2.16E-05	2.78E-07		3.08E-07	
ER-EC-11_m1-2	5/18/2010	9.80E-07	2.35E-08	7.96E-07	1.59E-08	1.79E-07	3.57E-09
ER-EC-6_m1-4	2/10/2000	1.01E-06	2.02E-08	6.51E-07		2.57E-07	
ER-EC-12_m1	3/26/2012	1.05E-06	3.49E-08	1.41E-07	2.82E-09	4.34E-07	8.68E-09
ER-EC-12_m2	7/20/2016	1.18E-06	1.86E-08	6.92E-07	1.39E-08	2.14E-07	6.25E-09
ER-EC-1_m1-3	2/1/2000	9.80E-07	1.96E-08	3.44E-07		2.99E-07	
ER-EC-15_m1	2/17/2014	1.29E-06	2.02E-08	5.10E-06	1.02E-07	3.70E-07	7.40E-09
ER-EC-15_m2	1/10/2014	1.28E-06	1.26E-08	9.75E-07	1.95E-08	4.84E-07	9.67E-09
ER-EC-15_m3	11/5/2013	1.33E-06	9.96E-09	1.61E-06	3.22E-08	2.43E-07	4.87E-09
ER-EC-13_m1	3/29/2013	1.19E-06	2.53E-08	2.94E-07	5.88E-09	1.57E-07	3.15E-09
ER-EC-13_m2	7/12/2012	1.24E-06	2.74E-08	4.43E-07	9.85E-09	2.67E-07	9.71E-09
ER-EC-14_m1	5/12/2014	1.46E-06	3.28E-08	2.03E-07	4.05E-09	1.98E-07	3.94E-09
ER-EC-14_m2	4/6/2014	1.46E-06	3.30E-08	2.12E-07	4.24E-09	1.96E-07	3.91E-09
ER-EC-2A_m3	10/11/2016	1.29E-06	1.88E-08	2.14E-07	4.28E-09	1.42E-07	4.95E-09
ER-EC-5_m1-3	7/15/2003	1.60E-06	3.20E-08	2.26E-07		1.94E-07	
ER-EC-7_m1-2	7/21/2003	1.16E-06	2.32E-08	2.18E-07		2.00E-07	
ER-EC-4_m2-3	6/24/2003	1.41E-06	2.82E-08	5.25E-07		2.52E-07	
ER-EC-8_m1-3	9/29/2016	1.39E-06	3.90E-08	1.10E-07	2.20E-09	1.61E-07	4.69E-09

229 S11 E48 01 1 Beatty Wash Windmill Well_s1Q	11/11/1997	1.17E-06	2.34E-08	5.95E-07			
ER-OV-01_p1	11/8/1997	1.56E-06	3.12E-08	4.46E-07			
ER-OV-06a_p1	11/8/1997	1.60E-06	3.20E-08	4.46E-07			
ER-OV-03c_p1	11/10/1997	1.21E-06	2.42E-08	1.64E-07			
Tolicha Peak_o1	11/12/1997	2.48E-07	4.96E-09	2.12E-07			
ER-OV-05	11/7/1997						
ER-OV-02_p1	11/11/1997	2.08E-06	4.16E-08	2.20E-07			
ER-OV-03a_p1	11/9/1997	1.52E-06	3.04E-08	9.30E-08			
Goss Springs_g	11/13/1997	1.55E-06	3.10E-08	4.09E-08			
Spdale Upper Well_m1	11/12/1997	1.52E-06	3.04E-08	2.49E-07			
Hot Springs Bath House 1_s1	11/14/1997	2.39E-06	4.78E-08	4.84E-07			
ER-OV-04A_p1	11/7/1997	1.21E-06	2.42E-08	1.34E-07			
ER-18-2_m1	6/17/2003	2.77E-06	5.54E-08	6.81E-06		1.10E-07	
ER-30-1_m1	8/10/2017	9.95E-07	1.27E-08	6.58E-08	1.32E-09	1.86E-07	3.72E-09
UE-29a 2_p1	11/6/1997	1.64E-06	3.28E-08	4.09E-08			
J-13 WW_m2	5/13/1993			1.52E-07		1.66E-07	
J-12 WW_m1	5/13/1993			7.35E-08		1.67E-07	

Location Identifier	**date**	**Ar**	**Ar_unc**	**Kr**	**Kr_unc**	**Xe**	**Xe_unc**
ER-12-3_m1	5/1/2015	3.37E-04	6.73E-06	6.99E-08	2.10E-09	1.02E-08	3.44E-10
ER-12-4_m1	5/9/2015	2.67E-04	5.34E-06	6.06E-08	1.83E-09	1.03E-08	3.09E-10
UE-19c WW_m1	8/13/1992	2.82E-04		7.51E-08		1.15E-08	

ER-20-6-2_p1	11/27/1996	5.38E-04		9.07E-08		1.15E-08	
ER-20-6-3_p1	12/16/1996	5.23E-04		9.34E-08		1.18E-08	
U-20 WW_m1	11/5/1997	2.40E-04				8.79E-09	
U-20n PS 1D_o3Z	7/9/2003					1.13E-08	
ER-20-5-3_m1	11/15/2001					1.03E-08	
ER-EC-11_m1-2	5/18/2010	2.59E-04	5.21E-06	5.84E-08	1.75E-09	8.07E-09	2.42E-10
ER-EC-6_m1-4	2/10/2000	3.27E-04				8.52E-09	
ER-EC-12_m1	3/26/2012	4.31E-04	8.62E-06	8.16E-08	2.45E-09	1.14E-08	3.42E-10
ER-EC-12_m2	7/20/2016	2.87E-04	5.73E-06	6.10E-08	1.83E-09	8.15E-09	2.44E-10
ER-EC-1_m1-3	2/1/2000	3.39E-04				8.70E-09	
ER-EC-15_m1	2/17/2014	4.13E-04	8.30E-06	7.92E-08	2.37E-09	1.02E-08	3.07E-10
ER-EC-15_m2	1/10/2014	4.61E-04	9.26E-06	8.00E-08	2.40E-09	1.15E-08	3.43E-10
ER-EC-15_m3	11/5/2013	2.75E-04	5.51E-06	5.84E-08	1.75E-09	7.59E-09	3.13E-10
ER-EC-13_m1	3/29/2013	2.18E-04	4.35E-06	4.76E-08	1.43E-09	6.81E-09	2.04E-10
ER-EC-13_m2	7/12/2012	2.64E-04	5.27E-06	5.28E-08	1.58E-09	6.94E-09	2.08E-10
ER-EC-14_m1	5/12/2014	2.25E-04	4.50E-06	4.65E-08	1.40E-09	6.14E-09	1.84E-10
ER-EC-14_m2	4/6/2014	2.38E-04	4.76E-06	4.84E-08	1.45E-09	6.81E-09	2.04E-10
ER-EC-2A_m3	10/11/2016	1.98E-04	3.94E-06	4.46E-08	1.34E-09	6.10E-09	1.86E-10
ER-EC-5_m1-3	7/15/2003	2.43E-04		4.98E-08		7.28E-09	
ER-EC-7_m1-2	7/21/2003	2.76E-04		5.91E-08		8.27E-09	
ER-EC-4_m2-3	6/24/2003	2.66E-04		5.28E-08		7.32E-09	
ER-EC-8_m1-3	9/29/2016	1.95E-04	3.91E-06	4.05E-08	1.22E-09	5.47E-09	1.64E-10
229 S11 E48 01 1 Beatty Wash Windmill Well_s1Q	11/11/1997	2.37E-04				7.83E-09	
ER-OV-01_p1	11/8/1997	2.17E-04				7.19E-09	
ER-OV-06a_p1	11/8/1997	2.24E-04				8.23E-09	
ER-OV-03c_p1	11/10/1997	2.54E-04				6.97E-09	
Tolicha Peak_o1	11/12/1997	3.08E-04				9.39E-09	

ER-OV-05	11/7/1997	2.45E-04				7.69E-09	
ER-OV-02_p1	11/11/1997	2.43E-04				7.83E-09	
ER-OV-03a_p1	11/9/1997	2.93E-04				8.14E-09	
Goss Springs_g	11/13/1997	3.32E-04				8.02E-09	
Spdale Upper Well_m1	11/12/1997	2.61E-04				8.10E-09	
Hot Springs Bath House 1_s1	11/14/1997	2.17E-04				7.09E-09	
ER-OV-04A_p1	11/7/1997	2.70E-04				7.80E-09	
ER-18-2_m1	6/17/2003	1.31E-04		2.58E-08		4.02E-09	
ER-30-1_m1	8/10/2017	2.67E-04	5.32E-06	5.88E-08	1.77E-09	8.96E-09	2.69E-10
UE-29a 2_p1	11/6/1997	2.83E-04				8.61E-09	
J-13 WW_m2	5/13/1993	2.49E-04		5.38E-08		7.74E-09	
J-12 WW_m1	5/13/1993	2.58E-04				7.91E-09	

Table S3 Derived parameters

Location Identifier	model	Chi-squared Probability	NGRT [C]	NGRT_unc [C]	Dne [%]	DNe_unc [%]
ER-12-3_m1	UA	0.11	16.2	0.8	67	3
ER-12-4_m1	UA_noXe	0.32	20.8	1	12	2
UE-19c WW_m1	UA_noNe	0.00	12.4	1.1	-15	2
ER-20-6-2_p1	UA_noAr	0.64	12.6	0.9	171	6
ER-20-6-3_p1	UA	0.02	12.1	0.8	212	7
U-20 WW_m1	UA	0.00	21.5	1.5	0	
U-20n PS 1D_o3Z	UA	0.00	10.5	0.9	36	3
ER-20-5-3_m1	UA	0.00	14.7	1	87	4
ER-EC-11_m1-2	UA	0.11	22	0.8	15	2
ER-EC-6_m1-4	UA	0.18	19.6	0.9	62	3
ER-EC-12_m1	UA	0.11	14.6	0.8	162	6
ER-EC-12_m2	UA	0.91	21.4	0.8	37	4
ER-EC-1_m1-3	UA	0.80	20.3	0.9	89	4
ER-EC-15_m1	UA	0.21	15.4	0.8	125	5
ER-EC-15_m2	UA_noKr	0.57	13.9	1	190	6
ER-EC-15_m3	UA	0.11	26	1.1	61	3
ER-EC-13_m1	UA_noXe	0.21	31.5	1.2	8	2
ER-EC-13_m2	UA_noNe	0.48	27.3	1.4	78	7
ER-EC-14_m1	UA	0.01	33.8	1	38	3
ER-EC-14_m2	UA_noXe	0.70	32.3	1.3	35	3
ER-EC-2A_m3	UA_noAr	0.13	31.3	1	-3	3
ER-EC-5_m1-3	UA_noXe	0.78	30.7	1.2	32	3
ER-EC-7_m1-2	UA	0.29	21.7	0.8	28	3
ER-EC-4_m2-3	UA_noXe	0.39	32.1	1.4	73	4

ER-EC-8_m1-3	UA_noXe	0.19	40.7	1.5	17	3
229 S11 E48 01 1 Beatty Wash Windmill Well_s1Q	UA	0.00	24	1.4	0	
ER-OV-01_p1	UA	0.00	28.2	1.6	0	
ER-OV-06a_p1	UA	0.00	25.3	1.6	0	
ER-OV-03c_p1	UA	0.00	26.3	1.4	20.1	
Tolicha Peak_o1	UA	0.00	16.3	1.2	21	
ER-OV-05	UA	0.00	23.6	1.4	0	
ER-OV-02_p1	UA	0.00	23.6	1.4	0	
ER-OV-03a_p1	UA	0.00	21.7	1.3	38.4	
Goss Springs_g	UA	0.00	24.5	1.5	104.9	
Spdale Upper Well_m1	UA	0.00	21.3	1.3	0	
Hot Springs Bath House 1_s1	UA	0.00	29.2	1.6	0	
ER-OV-04A_p1	UA	0.00	22.7	1.3	12.7	
ER-18-2_m1	UA_noXe	0.03	63.6	1.6	-4	2
ER-30-1_m1	UA_noXe	0.47	22.6	1.1	20	2
UE-29a 2_p1	UA	0.00	19	1.2	6.7	
J-13 WW_m2	UA	0.06	25.3	0.8	4	2
J-12 WW_m1	UA	0.16	23.8	0.9	3	2
Model						
UA: Unfractionated Excess Air						
UA_noNe: Outlier neon value excluded from fit						
UA_noAr: Outlier argon value excluded from fit						
UA_noKr: Outlier krypton value excluded from fit						
UA_noXe: Outlier xenon value excluded from fit						

Location Identifier	4He_ter / 4He_eq [-]	4He_ter / 4He_eq _unc [-]	R_ter / R_A [-]	R_ter/R_A _unc [-]	DNe_source	Dissolved Oxygen [mg/L]
ER-12-3_m1	21.88	0.47	0.01	0	measured	2.1
ER-12-4_m1	0.95	0.05	0.08	0.05	measured	-
UE-19c WW_m1	7.57	0.23			measured	-
ER-20-6-2_p1	1.58	0.12			measured	-
ER-20-6-3_p1	2.98	0.15	0.03	2.4	measured	-
U-20 WW_m1	3.52	0.16	0.11	0.05	model	4.6
U-20n PS 1D_o3Z	8.25	0.2			measured	-
ER-20-5-3_m1	5.07	0.15			measured	4.2
ER-EC-11_m1-2	19.27	0.41	0.52	0.15	measured	3.2
ER-EC-6_m1-4	14.97	0.34	0.7	0.02	measured	3.5
ER-EC-12_m1	0.65	0.1	0.01	0.69	measured	1.9
ER-EC-12_m2	16.34	0.36	0.84	0.03	measured	2.9
ER-EC-1_m1-3	6.79	0.18	0.62	0.03	measured	4.4
ER-EC-15_m1	128.18	2.62	0.93	0.03	measured	1.6
ER-EC-15_m2	21.66	0.5	0.91	0.03	measured	2
ER-EC-15_m3	39.65	0.83	0.96	0.03	measured	3.8
ER-EC-13_m1	6.51	0.15	0.84	0.04	measured	5.2
ER-EC-13_m2	9.95	0.28	0.88	0.04	measured	3.7
ER-EC-14_m1	3.88	0.11	1.08	0.05	measured	3.5
ER-EC-14_m2	4.11	0.11	1.08	0.05	measured	3.5
ER-EC-2A_m3	4.54	0.12	0.92	0.04	measured	4
ER-EC-5_m1-3	4.49	0.12	1.1	0.1	measured	5.2
ER-EC-7_m1-2	4.3	0.12	0.77	0.03	measured	4.4

ER-EC-4_m2-3	11.73	0.27	1.02	0.03	measured	3.4
ER-EC-8_m1-3	1.73	0.07	0.39	0.85	measured	4.8
229 S11 E48 01 1 Beatty Wash Windmill Well_s1Q	14.28	0.33	0.84	0.03	model	1.2
ER-OV-01_p1	10.47	0.26	1.13	0.04	model	4.9
ER-OV-06a_p1	10.46	0.26	1.16	0.04	model	4.6
ER-OV-03c_p1	3.01	0.15	0.83	0.06	model	4.8
Tolicha Peak_o1	4.18	0.18	0.01	0.02	model	5.7
ER-OV-05					model	6.3
ER-OV-02_p1	4.66	0.17	1.61	0.07	model	4.8
ER-OV-03a_p1	0.94	0.15	1.25	0.25	model	6.3
Goss Springs_g	0	0.03			model	7.4
Spdale Upper Well_m1	5.39	0.18	1.11	0.05	model	5.8
Hot Springs Bath House 1_s1	11.43	0.27	1.79	0.06	model	-
ER-OV-04A_p1	2.29	0.15	0.82	0.08	model	5.3
ER-18-2_m1	173.72	3.49	2.01	0.06	measured	1.2
ER-30-1_m1	0.49	0.04	0.06	0.08	measured	-
UE-29a 2_p1	0	0.03			model	-
J-13 WW_m2	2.84	0.08			measured	4.8
J-12 WW_m1	0.83	0.05			measured	5.2